NUCLEAR ENERGY RESEARCH INITIATIVE (NERI)

FINAL REPORT

Near-Core and In-Core Neutron Radiation Monitors for Real Time Neutron Flux Monitoring and Reactor Power Level Measurements

Grant Number DE-FG03-02SF22611

No. 2002-174

Final Report

Submitted by:

Lead Organization: (Kansas State University)

Douglas S. McGregor

Collaborating Organization(s): (None)

Submitted on:

June 12, 2006

NERI Final Report

Near-Core and In-Core Neutron Radiation Monitors for Real Time Neutron Flux Monitoring and Reactor Power Level Measurements

Grant Number DE-FG03-02SF22611
No. 2002-174

Design Concept

MPFDs are a new class of detectors that utilize properties from existing radiation detector designs. A majority of these characteristics come from fission chamber designs. These include radiation hardness, gamma-ray background insensitivity, and large signal output. However, one of the most significant differences from fission chambers is the detector size. Because of this, characteristics and fabrication methods of semiconductor detectors have been utilized to shrink fission chamber dimensions down and form MPFDs [13].

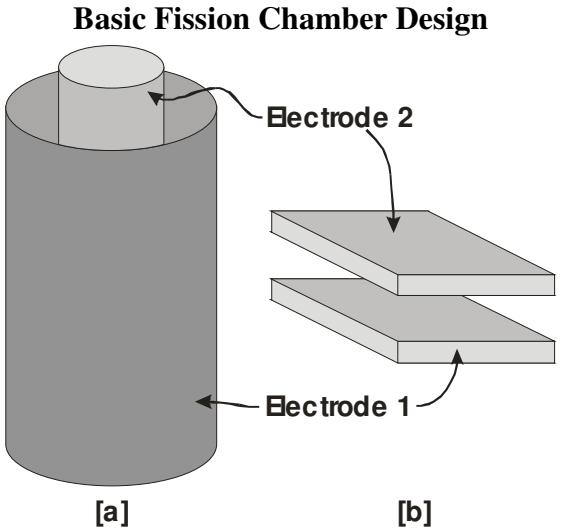

Figure 1: Basic design of [a] cylindrical and [b] parallel plate fission chambers.

Fission chambers are defined by their shape, their fissile coatings, and their mode of operation. The first of these characteristics, the shape, can be described as either cylindrical or parallel plate. The cylindrical construction is the most common and is made from a cylindrical tube and a center wire or a smaller cylindrical tube (Figure 1a). These two surfaces become the two electrodes across which a bias voltage is applied. The bias, from 50 volts to thousands of volts, is kept from shorting by a resistive fill gas that occupies the space between the electrodes [2,3]. The parallel plate fission chamber is similar to the cylindrical fission chamber with the exception that the cylinders are replaced by two flat parallel surfaces (Figure 1b). This design change greatly affects the directional sensitivity of the fission chambers since the solid fissile materials are typically coated on one or both of the electrodes. Due to this, the cylindrical chambers have a symmetrical response to flux at right angles to the chamber axis, whereas the parallel plate chambers are directionally biased to flux beams normal to the coated electrode [3].

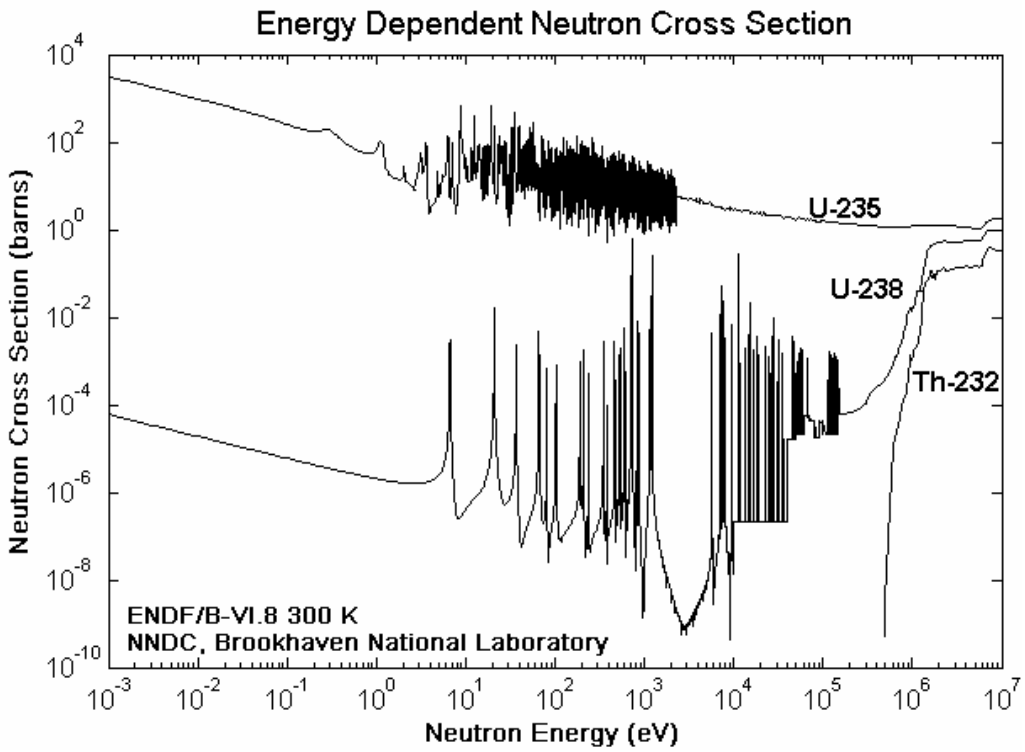

Figure 2: Energy dependent neutron cross sections for ^{235}U, ^{238}U, and ^{232}Th from the ENDF/B-VI.8 300 K cross section library [17].

The greatest change in detector performance is made by the fissile coating. This coating is commonly made from ^{235}U, ^{238}U, and ^{232}Th. Breeder coatings made from fertile isotopes may also be incorporated to extend the fission chamber's life. The sensitivity of a material to the energy of a neutron is defined by the material's neutron cross section. As the neutron cross section increases, the probability of an interaction also increases. For example, Figure 2 indicates that ^{235}U is primarily sensitive to slow (or low energy) neutrons, while ^{238}U and ^{232}Th are primarily sensitive to fast (or high energy) neutrons. Combinations of different isotopes and/or changing the coating thickness may be used to adjust the fission chamber for the desired operating sensitivities [2,3].

The fissile coating and the mode of operation are tightly coupled characteristics of fission chambers. The different modes of operation for fission chambers include pulse-mode, current-mode, and mean-square-voltage (MSV) mode. Pulse-mode operation counts every event which produces a voltage signal above a set threshold. This requires especially low neutron interaction efficiency for in-core detectors that are to be operated at full power. Most pulse-mode detectors are limited to 10^3 to 10^4 counts per second while the neutron flux at full power may be in excess of 10^{12} n cm^{-2} s^{-1}. Due to this, many higher efficiency fission counters will operate in pulse-mode at low powers and then switch to either current-mode or MSV mode at higher powers. Current-mode operation is the state where there are so many events that no individual event can be distinguished and the output signal appears as a constant current that is proportional to the neutron flux [2,3]. Offsets are inherent in current-mode signals due to the current production from background radiation. Current-mode signals are also affected by temperature, which introduces a drift in the signal. MSV, also known as Campbelling, attempts to remove these current-mode signal distortions by blocking the dc current component and analyzing the signal

variance, or mean of the squares of the deviations from the mean. This is possible since the time distribution of neutron interactions in the detector is a Poisson distribution and thus the number of events can be calculated based on the variance of the signal [2-3,18]. This mode of operation has the advantage of increased gamma discrimination, lowered temperature drifting, and allows a wider band of detector operation [18].

In addition to the three characteristics that define different types of fission chambers, there are some common features between them. Since they all utilize fission products for fill gas ionization, the neutron induced signals are far greater than the gamma ray background induced signals. This difference allows fission chambers to be relatively insensitive to the gamma-ray background. The materials used to construct the fission chambers are typically radiation hard and can withstand the extreme neutron and gamma radiation fields found in a reactor core. The design also allows the detectors to be used in high temperature environments [2,3].

The Basic MPFD Design

Micro-Pocket Fission Detectors utilize the general design concept of parallel plate fission chambers. They are made from three substrates, or ceramic plates, as shown in Figure 3. The substrates may be made from virtually any type of insulative material which has a low neutron absorption cross section, such as alumina (Al_2O_3) or oxidized silicon wafers. These substrates must also be capable of withstanding the temperature, chemical and radiation environments that the detectors will be deployed in. In order to fabricate the detectors, the two device-side substrates must have a metal coating to provide the two electrodes. These electrodes may be applied to the substrates by using common semiconductor processing techniques such as physical vapor deposition (PVD or evaporation), sputtering, or screen printing. One or both of these electrodes may then be coated with a neutron reactive material such as ^{10}B, ^{6}Li, ^{235}U, ^{238}U, and ^{232}Th. The third, or center, substrate must simply have a hole through it, which produces the chamber of the detector. When these substrates are sealed together (Figure 4), a fill gas is trapped in the chamber [1,13].

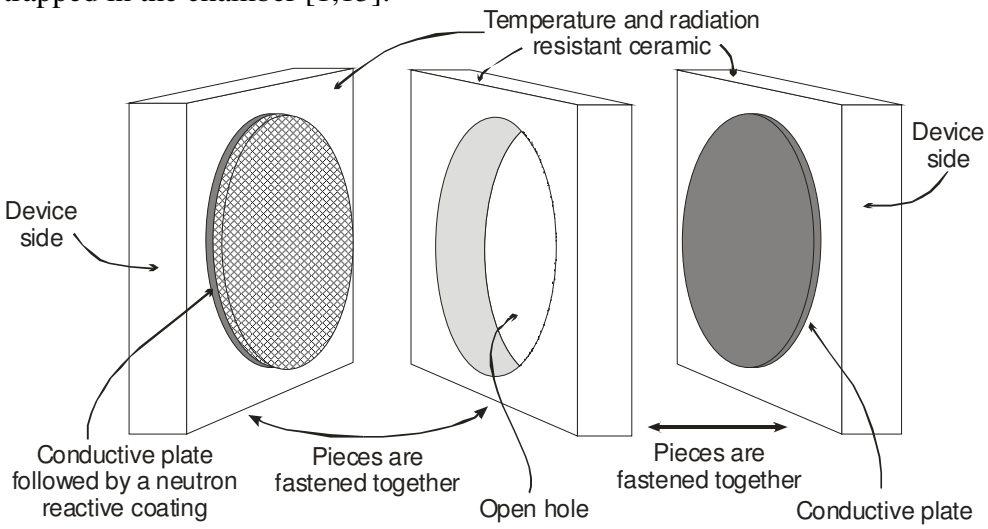

Figure 3: Basic construction method for fabricating MPFDs [13].

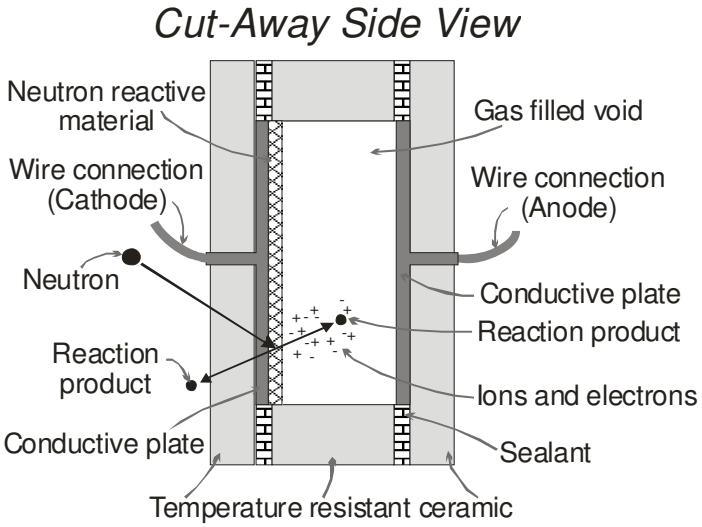

Figure 4: Cut-away side view of the MPFD showing fill gas ionization from a neutron induced reaction with the neutron reactive material [13].

What sets MPFDs apart from other fission chambers is that MPFDs do not rely on the full energy deposition from the fission products. This allows MPFDs to have a small chamber width and a low fill gas pressure while still being able to capture enough energy to distinguish neutron reactions from those of background radiation. Even with chamber widths of only 500 μm, MPFDs will capture approximately 3 MeV of energy from the fission products, compared to less than 500 eV for gamma rays [13]. Their small size also lends them to be able to sweep out charges quicker than other fission chambers since the charges have significantly less distance to travel. This allows the detectors to potentially achieve count rates greater than most fission chambers can achieve.

Most importantly, the miniature size allows multiple detectors to be placed where no other single fission chamber could fit, such as between fuel pins in a reactor core. In addition, their radiation hardness allows them to be placed in environments where other small detectors, such as semiconductors, would not survive.

The following chapters will expand this generalized design and show the full development of working MPFDs.

THEORETICAL DEVELOPMENT

This chapter investigates several theoretical principles behind the operation and design of the Micro-Pocket Fission Detectors. These principles include the energy deposition of neutron-induced reactions and its comparison to energy deposition from background radiation such as gamma-rays and electrons. Analysis is also shown for determining the maximum pulse-mode count rates the detectors may be capable of achieving. This information is then utilized to determine the desired neutron reactive coating thicknesses to be applied to the detectors. The chapter concludes with an investigation of the techniques utilized to optimize the neutron reactive coatings for flattened response and extended life.

Energy Deposition from Neutron-Induced Reactions

There are several possible coatings available to make ionization chambers sensitive to neutrons. The principle requirement is that the coating materials absorb neutrons and emit reaction products, preferably charged particles, which will ionize the fill gas. This requirement, along with the need to discriminate gamma ray (γ) and X-ray background from neutron interactions, excludes all (n,γ), (n,X-ray), and (n,n) reactions. Further, charged particles with large masses and high energies will deposit greater energies in the fill gas than energetic photons, thus producing larger signals than the expected background. As an additional requirement, the charged particle should be a prompt emission in order to provide a real-time response to neutron interactions.

Based on the conservation of energy, the Q value defines the combined neutron threshold energy required to cause a reaction along with the energy sum of the reaction products. In other words, the Q value is the amount of kinetic energy gained in a reaction. Based on Einstein's equation $E = mc^2$, the gain in kinetic energy must come from a decrease in the rest mass [4]. Therefore, if the Q value is negative then the reaction is endothermic and thus requires the neutron to have a minimum threshold energy before the reaction will take place. An exothermic reaction, or positive Q, will occur at any neutron energy and is therefore recommended, especially when working with slow neutrons. Several commonly used candidate coating materials that meet the criteria of prompt charged particle ejection and exothermic reactions are ^{10}B, ^{6}LiF, pure ^{6}Li, ^{235}U, ^{238}U, and ^{232}Th [1,13].

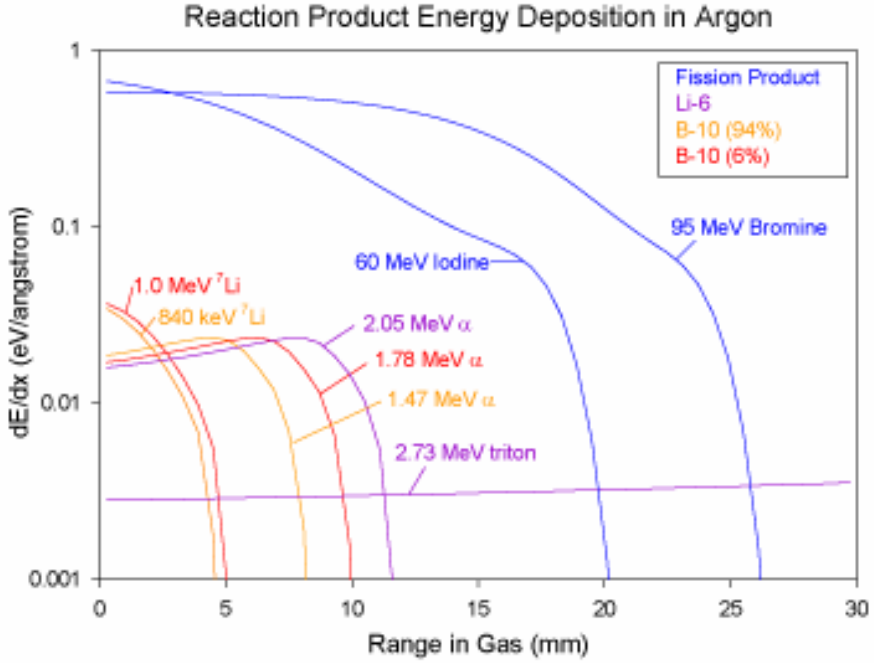

Figure 1: Energy deposition and range of neutron reaction products in argon fill gas at 1 atm.

^{10}B produces a 1.47 MeV α-particle and an 840 keV ^{7}Li ion in 94% of its neutron reactions and a 1.78 MeV α-particle and a 1.0 MeV ^{7}Li ion the other 6% of the neutron reactions. The Q value for the ^{10}B(n,α)^{7}Li reaction is 2.78 MeV. ^{6}LiF and pure ^{6}Li will undergo a ^{6}Li(n,α)^{3}H reaction producing a 2.05 MeV α-particle and a 2.73 MeV triton (^{3}H) with a Q value of 4.78 MeV [13,16]. The neutron induced fission process used by heavy nuclides such as ^{235}U, ^{238}U, and ^{232}Th creates two smaller prompt fission products with high energies along with several

prompt and delayed neutrons, gamma rays, and beta particles. The kinetic energy of some example fission products are 60 MeV Iodine and 95 MeV Bromine.

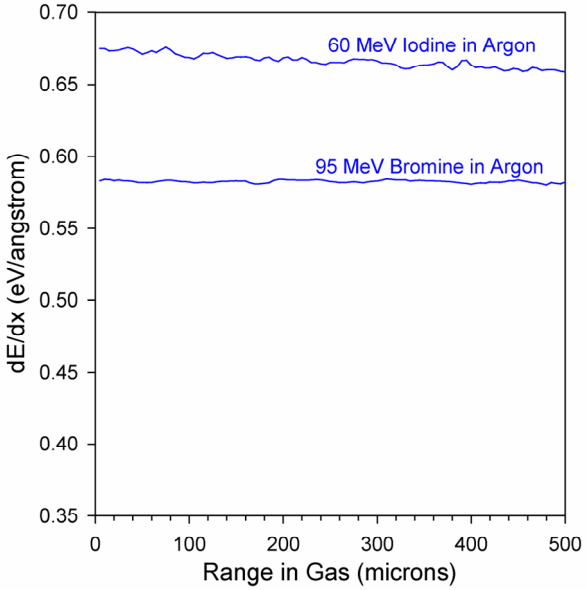

Figure 2: Expanded view of Figure 1 showing that nearly 3 MeV is deposited by fission products in only half a millimeter of argon fill gas at 1 atm.

Table 1: Energy deposition in the first 500 µm of argon fill gas at 1 atm for full energy reaction products.

Reaction Product	Energy (keV)
60 MeV Iodine	3332
(in P-10 fill gas)	*3295*
95 MeV Bromine	2911
(in P-10 fill gas)	*2880*
1.0 MeV ^{7}Li ion	180
840 keV ^{7}Li ion	168
1.47 MeV α-particle	94
1.78 MeV α-particle	86
2.05 MeV α-particle	80
2.73 MeV triton (^{3}H)	14

Calculation of the energy deposition and ranges of the neutron reaction products for ^{10}B and ^{6}Li along with representative fission products from ^{235}U, ^{238}U, and ^{232}Th in a 1 atm argon fill gas has been completed and is shown in Figure 1 [19]. The fission products show significantly higher energy deposition per unit distance of travel than the reaction products of ^{10}B and ^{6}Li. The higher dE/dx of the fission products is desired in order to easily distinguish the neutron induced events from the background radiation. In fact, when considering the initial 500 µm of travel from full energy fission products, the dE/dx is nearly constant, and when integrated, the energy deposited is approximately 3 MeV (Figure 2). The integrated values for all the fissionable materials are tallied in Table 1.

Gamma-ray and Electron Insensitivity

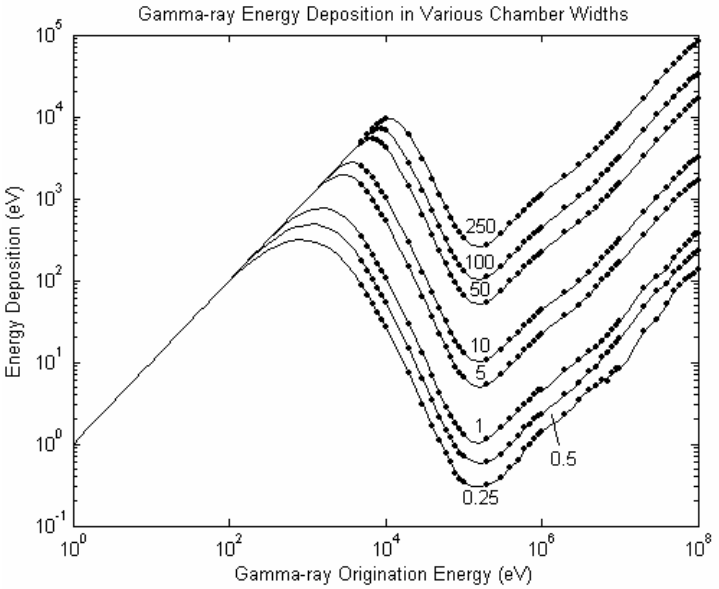

Figure 3: Data (dots) and spline fit (lines) of gamma-ray energy deposition in various chamber widths of argon gas.

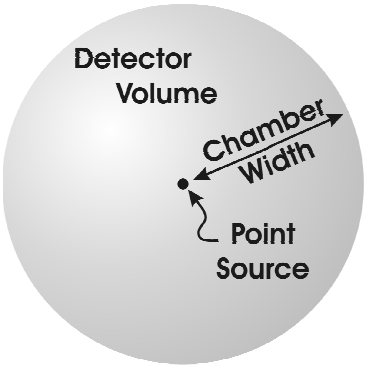

Figure 4: Geometry of MCNP energy deposition problem.

While it has been shown in the previous section that fission products will deposit large amounts of energy in microscopic distances, it must also be shown how much energy will be deposited by other charged particles in the same chamber. These charged particles exist as background from the core but may also be emitted inside the chamber from the decay of the fission products in the form of photons (gamma rays, X-rays, and bremsstrahlung radiation) and electrons (beta particles). To determine the energy deposition of this background radiation, a series of Monte Carlo simulations was completed using MCNP [20]. The basic simulation was set up using an isotropic point source surrounded by an argon spectroscopy (F7*) detector sphere as depicted in Figure 4. One million histories were tested to find the energy deposition through eight different chamber widths. Gamma ray energies ranging from 5 keV to 100 MeV and electrons from 5 keV to 10 MeV were tested through this MCNP code. Once collected, the data underwent a spline fit analysis to determine the maximum reasonable deposition energy for each

chamber width. The reasonable level has been set to origination energies less than 10 MeV. Plots from this analysis are presented in Figures 3 and 5 with the numerical results listed in Table 2.

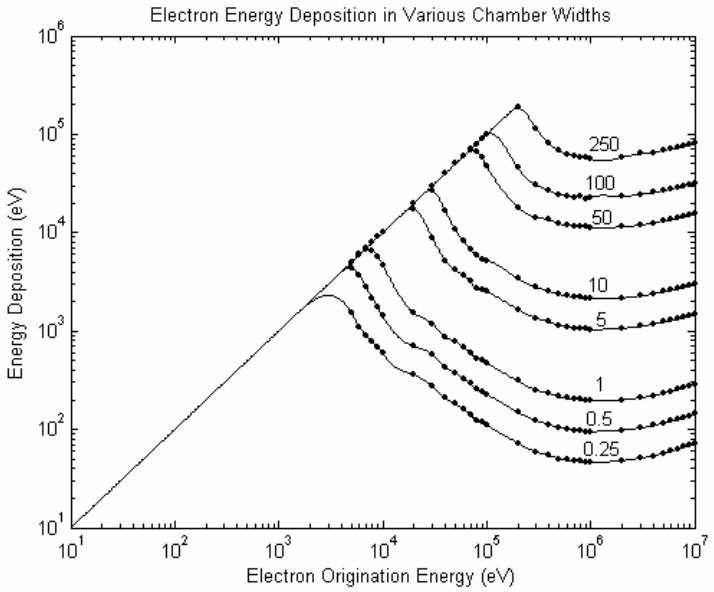

Figure 5: Data (dots) and spline fit (lines) of gamma-ray energy deposition in various chamber widths of argon gas.

Table 2: Gamma-ray and electron average energy deposition in 1 atm argon for various chamber widths.

Chamber Width (mm)	Gamma-ray		Electron	
	Origination Energy (eV)	Energy Deposition (eV)	Origination Energy (eV)	Energy Deposition (eV)
0.25	843.6	312.2	3000	2316
0.50	1135	485.6	4805	4370
1.00	1522	754.3	7357	6721
5.00	2919	1954	19140	17660
10.0	3768	2772	28730	26790
50.0	6628	5416	73690	68940
100.0	8437	7015	108500	102200
250.0	11360	9646	199500	186200

When this data is compared to the energy deposition from fission products, as shown in Figure 6, one should quickly see how insignificant gamma-ray and electron events are compared to the neutron reactions. While the gamma-ray and electron energy deposition appears to be negligible for all chamber sizes, it must be remembered that the probability of interaction increases with increasing chamber volume. Therefore, the integrated signal contribution from the background radiation will become comparable to the neutron induced events. Because of this problem, many fission chambers must take this into account when reporting neutron fluxes, especially when operated in current-mode. Figure 6 further illustrates that even with small chamber widths, the neutron induced signal will be far greater than the background induced

signals, which, when interaction probabilities are taken into account, show smaller fission chambers are, in fact, superior to large fission chambers.

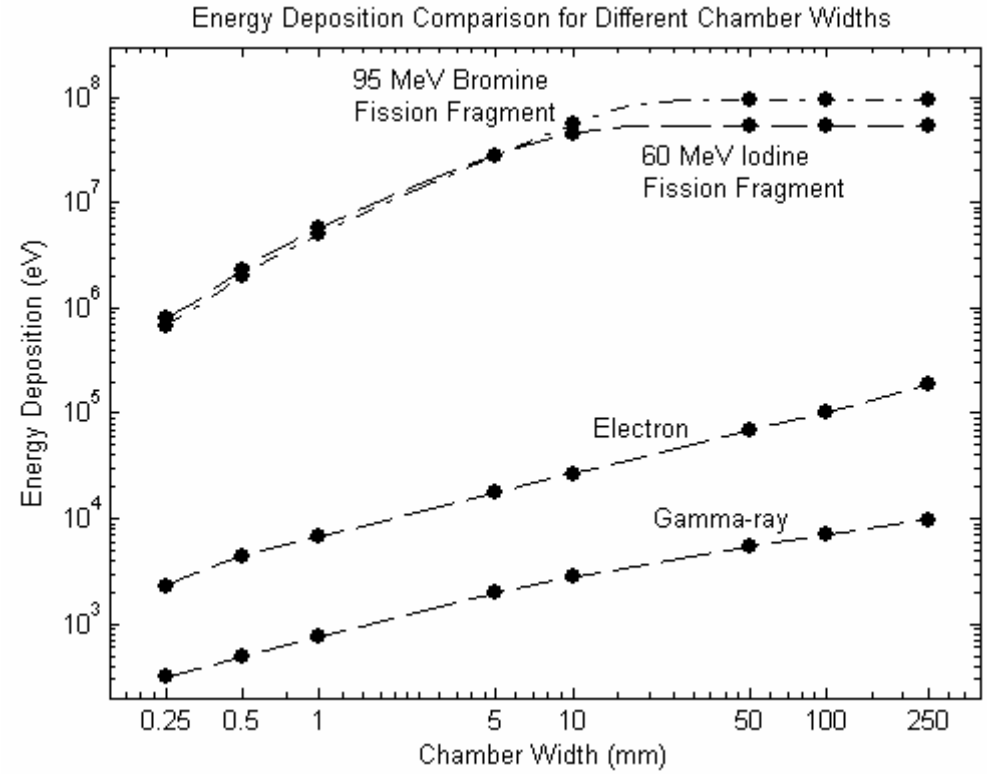

Figure 6: Energy deposition comparison for different chamber widths.

Saturation Level

The point at which a detector enters a saturated state is dependent on the time it takes the detector to clear the ions and electrons after an event. This time is dependent on the mobilities of both the ions and electrons. Since the fission products from the neutron event will leave a trail of ionized gas as it passes through the chamber, the assumption that the ions and electrons must travel the full width of the chamber must be made. Therefore the time needed to sweep out the ions or electrons from the chamber can be defined as

$$t = \frac{w}{v} \tag{1}$$

where t is the time, w is the chamber width, and v is the ion or electron drift velocity. This drift velocity may be expanded as

$$v = \frac{\mu \mathcal{E}}{p} \tag{2}$$

with μ equal to the ion or electron mobility, $\mathcal{E}$ is the electric field applied to the detector chamber, and p is the pressure of the fill gas [2]. Knowing that the chamber is a constant volume, the ideal gas law may be applied to include temperature into the calculations. The electric field is also defined as the voltage over distance, or $\mathcal{E} = V/w$. Thus the drift velocity equation may be redefined as

$$v = \frac{\mu V T_1}{w p T_2}. \tag{3}$$

where T_1 and T_2 are the reference temperature and the new temperature, respectively.

Since the mobility is specific for every gas and mixture, the fill gas must be defined to complete this analysis. Possible fill gases include, but may not be limited to, Ar, Xe, Ne, He, Carbon Dioxide (CO_2), Methane (CH_4), Ethane (C_2H_6), Propane (C_3H_8), Isobutane (C_4H_{10}), Methylal ($CH_3OCH_2OCH_3$), and Dimethyl Ether (DME), along with any mixture of these chemicals [21]. The addition of a quenching gas to a noble gas is often used to control multiplication of ionization in the fill gas. However, the molecular quenching gases will decompose in radiation fields and thus age the detector [22]. The chemically active molecules formed in the amplifying avalanche can damage the detector. A pure noble gas, such as Ar, is monatomic and thus will not decompose and thus will not age [22]. Since the MPFDs will be used in high radiation fields, pure Ar has been chosen as the fill gas. In addition, since the energy deposition is very large and we are only interested in counting events, not spectroscopy, the detectors do not need high gain or good proportionality. With this decision made, the ion sweep out time can be determined.

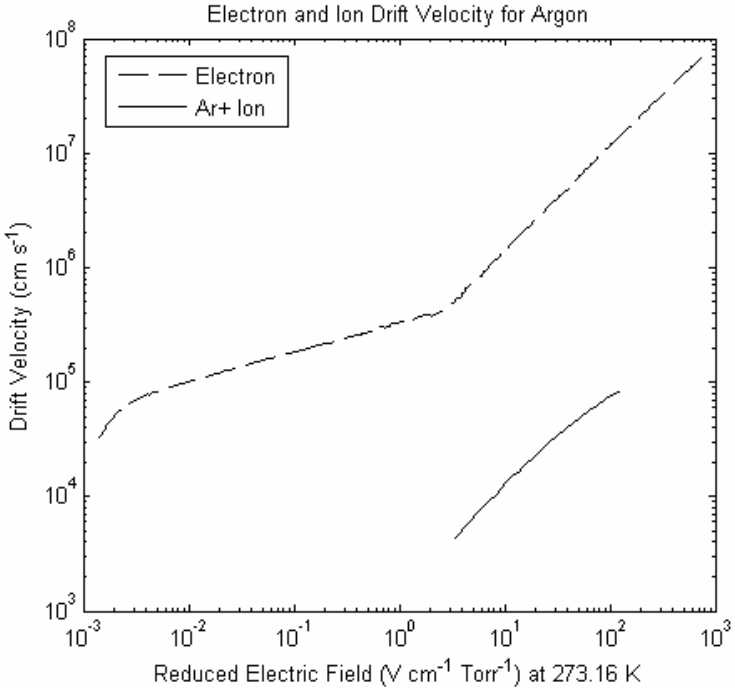

Figure 7: Drift velocity of electrons and Ar+ ions in argon at 273.16 K [23,24].

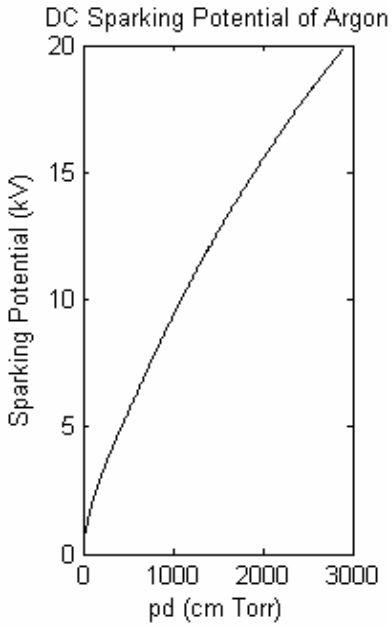

Figure 8: DC sparking potential of argon as a function of pressure and chamber width [25].

The drift velocities of electrons and Ar+ ions in argon were collected from Biagi and Johnsen, respectively, and converted to similar scales (Figure 7) [23,24]. The reduced electric field $(\mathcal{E}/p)$ scale was set at 1 Torr and 273.16 K (0°C). Another factor that must be taken into account when using this data is at what point the applied bias will cause the argon to break down and produce an arc across the chamber. Data for this is reproduced and shown in Figure 8.

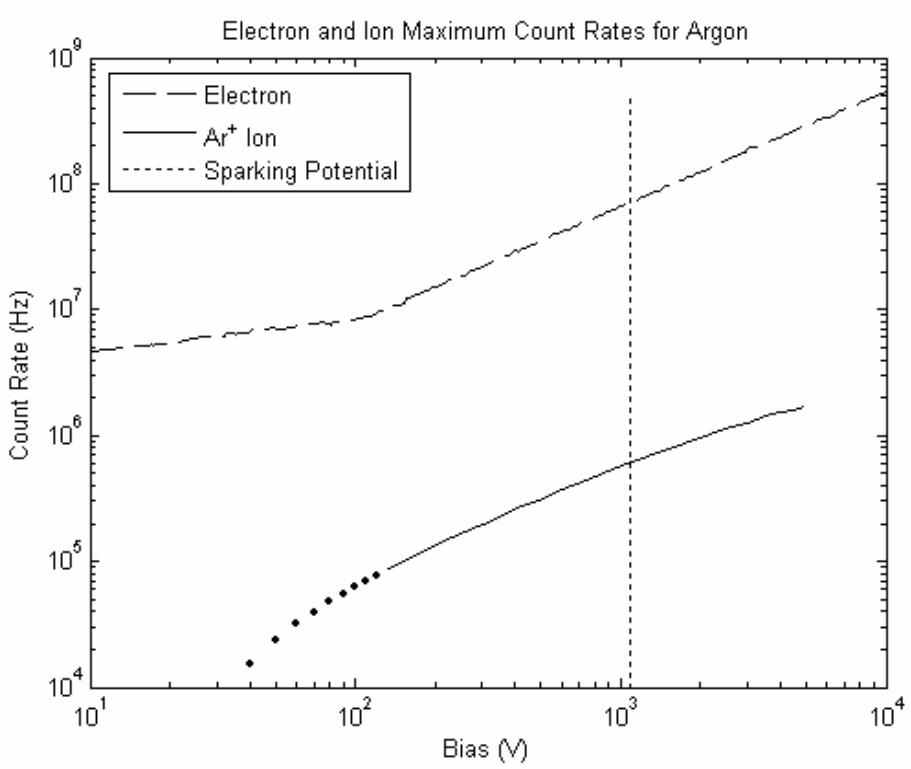

Figure 9: Maximum count rate achievable versus detector bias for pure argon fill gas.

With these sets of data, it is now possible to calculate the depletion time for the electrons and ions. However, of greatest interest is the maximum count rate that may be achieved by the detectors, which is simply the inverse of the time. For further definition of the problem, it is assumed that the chambers will all be filled with 1 atm (760 Torr) of pure argon gas at 25°C, the typical room temperature of where the detectors are assembled. The average temperature that these detectors will be operated in is approximately 35°C for the Kansas State University TRIGA Reactor. The chamber width has also been set to 500 μm for these calculations. Figure 9 shows the calculated maximum count rate results. From these results, the detector should be able to record nearly 63,000 events with a bias of 100 V and up to 200,000 events with a bias slightly greater than 300 V.

While these numbers are remarkable and show that these devices are quite fast, several other factors must be taken into consideration. The most basic factor is that this count rate is dependent on synchronous events, thus the neutron interactions must occur at a precise rate, and no event occurs until the last ion has cleared the chamber. Radiation does not behave this way, as it is stochastic, or asynchronous, in nature. Therefore, while an average rate will be attained, the rate of interactions will vary between every pair of interactions. To compensate for the stochastic nature of radiation, the maximum count rate will be assumed to be half of the predicted value.

Another factor that greatly influences the speed of the detection system is the amplification circuitry. However, since this can be designed around the characteristics of the detector, such discussion will be deferred.

A third factor affecting the maximum count rate is the purity of the argon fill gas. Brown presents electron drift velocity comparisons of both pure argon and industrial grade argon [25]. In these comparisons the industrial grade argon electron drift velocity is approximately 5/12 of

the pure argon [25]. While there is no similar data for argon ions, which will determine the maximum detector count rate, the same trend for conservative count rate suppression, due to impurities in the fill gas, has been applied.

Using an experimentally determined best operating bias of 200 V, along with the above suppression factors, the maximum count rate is approximately 28 kHz. This maximum count rate value may now be utilized to determine the proper neutron reactive coating thickness.

Fissile Coating Thickness and Lifetime

High Z fissile coatings have shown to produce the optimal neutron reaction signals due to the high output signals. However, to remain in pulse-mode the reactive coating thickness must be determined so as to not enter saturation prematurely. Analysis for the determination of this coating thickness is based on the fundamental reaction rate equation

$$R = \Sigma\phi \tag{4}$$

where Σ is the macroscopic neutron cross section (cm^{-1}) of the coating material and ϕ is the neutron flux density (cm^{-2} s^{-1}). The macroscopic neutron cross section is defined by tabulated microscopic cross section data, σ (barns), multiplied by the number of atoms per cm^3, N. Expanded, the reaction rate equation takes on the form

$$R = \Sigma\phi = \sigma N\phi = \sigma\frac{\rho N_a}{A}\phi = \sigma\frac{mN_a}{adA}\phi \tag{5}$$

with material density ρ (g cm^{-3}), atomic weight A (g mol^{-1}), and Avogadro's number N_a (atoms mol^{-1}). The density can further be expanded into the mass m (g), the surface area a (cm^2), and the coating thickness d (cm).

To find the necessary coating thickness one must first find the neutron flux at the desired operating power. Since the core of a nuclear reactor contains a continuous distribution of neutron energies, this energy profile should be characterized in order to properly determine the resulting reaction rate. The Kansas State University TRIGA Reactor core neutron flux energy profile was mapped experimentally through the use of a series of activation foils and a fission chamber [26]. While the method was able to roughly distinguish between slow, fast, and epithermal neutron energies, it is unable to resolve the true neutron energy profile [26]. Theoretical reconstruction of the flux profile with experimental support is required to be able to find the neutron flux over a small energy range ΔE. The total neutron profile can be described by separating it into three sections, the slow, epithermal, and fast regions. The flux ϕ_M at energy E in the slow region is normally approximated by a Maxwell-Boltzmann distribution as described by the equation

$$\phi_M(E) = \frac{2\pi n}{(\pi kT)^{3/2}}E^{1/2}e^{-E/kT} \tag{6}$$

where k is Boltzmann's constant (8.62 x 10^{-5} eV/K), T is the temperature (K), and n is a scaling factor [27]. A common method of shifting the Maxwellian distribution towards the actual distribution is done by shifting the flux profile by adjusting the temperature variable. Shifting the temperature helps take into account the complex matter interactions from the low-energy neutrons. A reasonable adjustment is to raise the temperature setting to 440 K [28].

The fast neutron spectrum has been found to be reasonably described by the formula

$$\phi_F(E) = 0.453ne^{-1.036E}\sqrt{\sinh(2.29E)} \tag{7}$$

for the energy range of about 0.18 to 12 MeV [27]. The epithermal region between the slow and fast regions satisfies the 1/E law. The slow and epithermal regions are assumed to join at 0.625 eV [27]. For the integrated neutron fluxes of the Kansas State University TRIGA Reactor, as listed in Table 3, the approximate energy dependent neutron fluxes of the three regions produces the profiles shown in Figure 10.

Table 3: Neutron flux for the Kansas State University TRIGA Reactor [29].

Location	Neutrons cm^{-2} s^{-1} at 250 kW	
	Fast (>10 keV)	Slow (<0.21 eV)
Central Thimble	1.2×10^{13}	1.0×10^{13}
E-Ring	6.4×10^{12}	4.1×10^{12}
F-Ring (Rabbit)	3.5×10^{12}	4.3×10^{12}

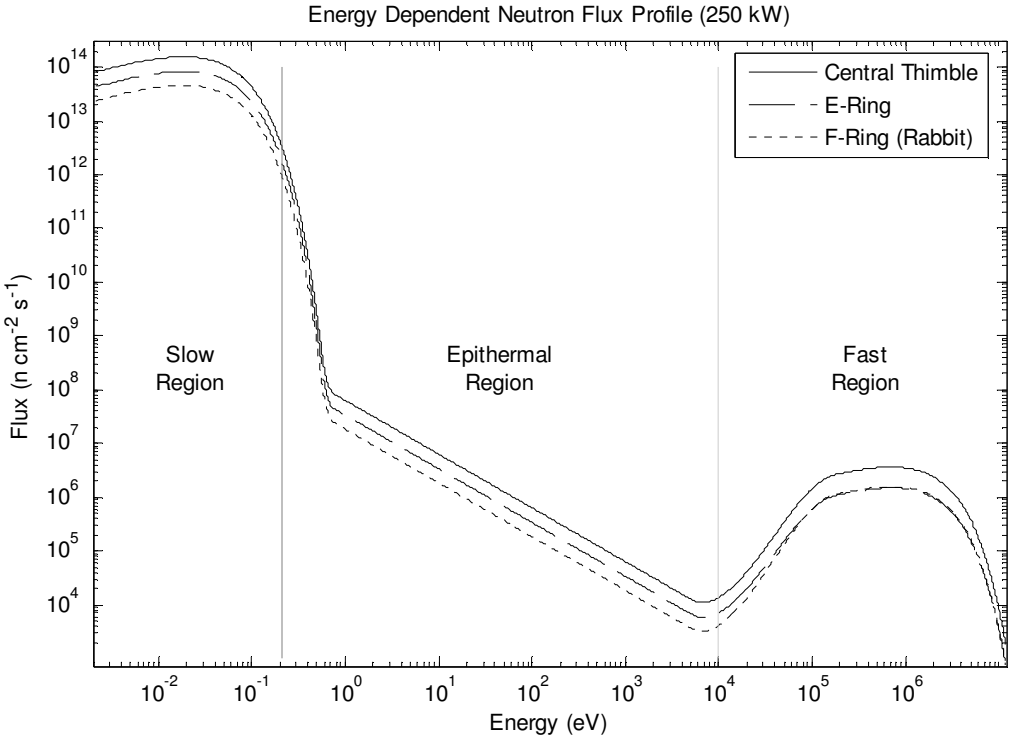

Figure 10: Energy dependent neutron flux profiles for the Kansas State University TRIGA Reactor in the Central Thimble, E-Ring, and F-Ring (see Error! Reference source not found. **for generation program).**

Integration of the energy dependent neutron flux profile is used for numerical verification through the equation

$$\int_{E_L}^{E_H} \phi(E)\,dE \tag{8}$$

where $\phi(E)$ is the flux at energy E with the lower cutoff energy E_L and upper cutoff energy E_H. The slow to epithermal transition energy is assumed to be 0.21 eV and the epithermal to fast transition energy is assumed to be 100 keV as defined by the Kansas State University TRIGA

Reactor Training Manual [29]. Results of this integration verifies the manual's data and is shown in Table 4.

Table 4: Integrated energy dependent reactor flux for central thimble at 250 kW.

Energy Range	Lower Boundary (eV)	Upper Boundary (eV)	Integrated Flux (n cm^{-2} s^{-1})
Full	0	∞	2.2118×10^{13}
Slow	0	0.21	1.0000×10^{13}
Epithermal	0.21	10,000	1.1767×10^{11}
Fast	10,000	∞	1.2000×10^{13}

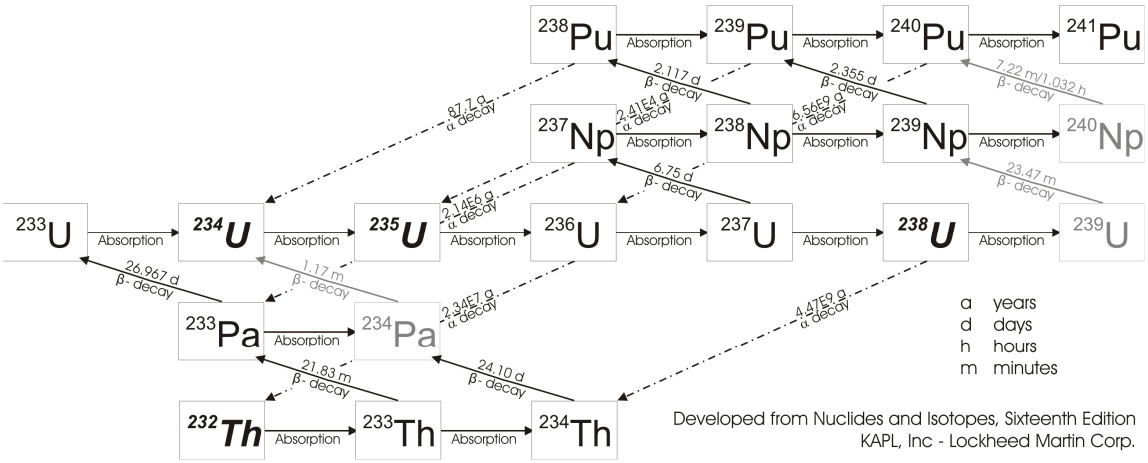

Figure 11: Isotope buildup and decay of fissile coatings (developed from [30]).

Using the calculated neutron flux profile it is possible to determine the reaction rate for a single atom of fissile material through Equation (5), and then the total number of atoms necessary to generate the desired reaction rate.

While the detectors are primarily sensitive to fission fragments from the fissile material, other interactions must be taken into consideration. The principle interaction of concern is neutron absorption since the resulting transmutation will buildup new fissile material with different cross section characteristics. In addition, the natural decay of the fissile material and the transmutated isotopes can buildup additional isotopes. Uranium and thorium fissile coatings will produce isotopes related to the buildup and decay scheme shown in Figure 11 with the resulting coupled ordinary differential equations

$$\frac{d\left[{}^{232}Th\right]}{dt} = \lambda_{{}^{236}U}\left[{}^{236}U\right] - A\left[{}^{232}Th\right] - F\left[{}^{232}Th\right] - \lambda_{{}^{232}Th}\left[{}^{232}Th\right] \tag{9}$$

$$\frac{d\left[{}^{233}Th\right]}{dt} = A\left[{}^{232}Th\right] - A\left[{}^{233}Th\right] - F\left[{}^{233}Th\right] - \lambda_{{}^{233}Th}\left[{}^{233}Th\right] \tag{10}$$

$$\frac{d\left[{}^{234}Th\right]}{dt} = A\left[{}^{233}Th\right] + \lambda_{{}^{238}U}\left[{}^{238}U\right] - A\left[{}^{234}Th\right] - F\left[{}^{234}Th\right] - \lambda_{{}^{234}Th}\left[{}^{234}Th\right] \tag{11}$$

$$\frac{d\left[{}^{233}Pa\right]}{dt} = \lambda_{{}^{233}Th}\left[{}^{233}Th\right] + \lambda_{{}^{237}Np}\left[{}^{237}Np\right] - A\left[{}^{233}Pa\right] - F\left[{}^{233}Pa\right] - \lambda_{{}^{233}Pa}\left[{}^{233}Pa\right] \quad (12)$$

$$\frac{d\left[{}^{233}U\right]}{dt} = \lambda_{{}^{233}Pa}\left[{}^{233}Pa\right] - A\left[{}^{233}U\right] - F\left[{}^{233}U\right] - \lambda_{{}^{233}U}\left[{}^{233}U\right] \quad (13)$$

$$\frac{d\left[{}^{234}U\right]}{dt} = A\left[{}^{233}Pa\right]^{*} + A\left[{}^{233}U\right] + \lambda_{{}^{238}Pu}\left[{}^{238}Pu\right] + \lambda_{{}^{234}Th}\left[{}^{234}Th\right]^{*} \quad (14)$$
$$\ldots - A\left[{}^{234}U\right] - F\left[{}^{234}U\right] - \lambda_{{}^{234}U}\left[{}^{234}U\right]$$

$$\frac{d\left[{}^{235}U\right]}{dt} = A\left[{}^{234}U\right] + \lambda_{{}^{239}Pu}\left[{}^{239}Pu\right] - A\left[{}^{235}U\right] - F\left[{}^{235}U\right] - \lambda_{{}^{235}U}\left[{}^{235}U\right] \quad (15)$$

$$\frac{d\left[{}^{236}U\right]}{dt} = A\left[{}^{235}U\right] + \lambda_{{}^{240}Pu}\left[{}^{240}Pu\right] - A\left[{}^{236}U\right] - F\left[{}^{236}U\right] - \lambda_{{}^{236}U}\left[{}^{236}U\right] \quad (16)$$

$$\frac{d\left[{}^{237}U\right]}{dt} = A\left[{}^{236}U\right] - A\left[{}^{237}U\right] - F\left[{}^{237}U\right] - \lambda_{{}^{237}U}\left[{}^{237}U\right] \quad (17)$$

$$\frac{d\left[{}^{238}U\right]}{dt} = A\left[{}^{237}U\right] - A\left[{}^{238}U\right] - F\left[{}^{238}U\right] - \lambda_{{}^{238}U}\left[{}^{238}U\right] \quad (18)$$

$$\frac{d\left[{}^{237}Np\right]}{dt} = \lambda_{{}^{237}U}\left[{}^{237}U\right] - A\left[{}^{237}Np\right] - F\left[{}^{237}Np\right] - \lambda_{{}^{237}Np}\left[{}^{237}Np\right] \quad (19)$$

$$\frac{d\left[{}^{238}Np\right]}{dt} = A\left[{}^{237}Np\right] - A\left[{}^{238}Np\right] - F\left[{}^{238}Np\right] - \lambda_{{}^{238}Np}\left[{}^{238}Np\right] \quad (20)$$

$$\frac{d\left[{}^{239}Np\right]}{dt} = A\left[{}^{238}U\right]^{*} + A\left[{}^{238}Np\right] - A\left[{}^{239}Np\right] - F\left[{}^{239}Np\right] - \lambda_{{}^{239}Np}\left[{}^{239}Np\right] \quad (21)$$

$$\frac{d\left[{}^{238}Pu\right]}{dt} = \lambda_{{}^{238}Np}\left[{}^{238}Np\right] - A\left[{}^{238}Pu\right] - F\left[{}^{238}Pu\right] - \lambda_{{}^{238}Pu}\left[{}^{238}Pu\right] \quad (22)$$

$$\frac{d\left[{}^{239}Pu\right]}{dt} = A\left[{}^{238}Pu\right] + \lambda_{{}^{239}Np}\left[{}^{239}Np\right] - A\left[{}^{239}Pu\right] - F\left[{}^{239}Pu\right] - \lambda_{{}^{239}Pu}\left[{}^{239}Pu\right] \quad (23)$$

$$\frac{d\left[{}^{240}Pu\right]}{dt} = A\left[{}^{239}Np\right]^{*} + A\left[{}^{239}Pu\right] - A\left[{}^{240}Pu\right] - F\left[{}^{240}Pu\right] - \lambda_{{}^{240}Pu}\left[{}^{240}Pu\right] \quad (24)$$

$$\frac{d\left[{}^{241}Pu\right]}{dt} = A\left[{}^{240}Pu\right] - A\left[{}^{241}Pu\right] - F\left[{}^{241}Pu\right] - \lambda_{{}^{241}Pu}\left[{}^{241}Pu\right]. \quad (25)$$

In these equations it has been assumed that the decay of ^{234}Pa, ^{239}U, and ^{240}Np is instantaneous. Absorption (A) and fission (F) reaction rates are based on the energy integration of the energy dependent flux profile and the respective absorption and fission cross sections per atom as defined by

$$A(t) = \int_{E_L}^{E_H} \sigma_A(E)\phi(E,t)\,dE \quad (26)$$

$$F(t) = \int_{E_L}^{E_H} \sigma_F(E)\phi(E,t)\,dE \quad (27)$$

The natural decay of the isotope is defined by

$$\lambda = \frac{\ln 2}{T_{1/2}} \tag{28}$$

where λ is the decay constant and $T_{1/2}$ is the half-life of the isotope. In order to properly perform the buildup and decay calculations it must be assumed that the reactor flux is held constant thus making A and F constants through time. All of the cross section data utilized by these programs is in discrete points and thus a linear trapezoidal rule is applied for integration, or

$$\int_{x_1}^{x_2} y dx = \frac{(y_2 - y_1)(x_2 - x_1)}{2} + (x_2 - x_1)\, y_1 \tag{29}$$

which may be reduced to

$$\int_{x_1}^{x_2} y dx = \frac{(y_2 + y_1)(x_2 - x_1)}{2}. \tag{30}$$

An ordinary differential equation solver routine in MATLAB is used to calculate the detectors' lifetime response instead of solving Equations (9) through (25) explicitly. The resulting solutions give a normalized number of atoms per original source atom of each isotope over time. Multiplying the normalized number of atoms by the fission reaction rate of that isotope is used to determine the resulting fission rate. Figures 12.0 through 17.0 show the resulting time dependent lifetime response of three different coatings (natural uranium, 93% enriched ^{235}U, and natural ^{232}Th) for the central thimble flux analysis. The resulting fission rate decrease over time and fluence is also tabulated in Table 6 for varying percentages of rate decrease. In order to achieve an initial count rate of 28,000 counts per second (as determined in Section 0) the coatings should be of the mass listed in Table 5. With the contact surface area defined, the coating thickness has been determined with Equation (5).

Table 5: Fissile coatings to achieve initial count rate of 28,000 s^{-1}.

Fissile Material	Coating Mass (g)	Coating Thickness (μm)
Natural Uranium	1.755×10^{-6}	11.36
93% enriched ^{235}U	1.489×10^{-8}	0.0964
^{232}Th	1.280×10^{-4}	1347

Table 6: Lifetime data for natural uranium, 93% enriched ^{235}U, and ^{232}Th fissile coatings for three flux levels.

Percent	Fluence (n cm^{-2})			Time (days)		
Loss	natural U	93% ^{235}U	^{232}Th*	natural U	93% ^{235}U	^{232}Th*
0.1%	5.56×10^{18}	3.70×10^{18}	9.64×10^{23}	2.9	1.9	504576
0.5%	8.20×10^{19}	1.85×10^{19}	1.44×10^{24}	42.9	9.7	752448
1%	1.88×10^{20}	3.71×10^{19}	1.44×10^{24}	98.2	19.4	753324
2%	3.85×10^{20}	7.46×10^{19}	1.44×10^{24}	202	39.1	755076
5%	9.20×10^{20}	1.90×10^{20}	1.45×10^{24}	481	99.2	760478
10%	1.75×10^{21}	3.89×10^{20}	1.47×10^{24}	914	204	769931
20%	3.54×10^{21}	8.25×10^{20}	1.51×10^{24}	1850	432	790444
30%	6.17×10^{21}	1.32×10^{21}	1.56×10^{24}	3230	690	813768
40%	5.52×10^{22}	1.89×10^{21}	1.61×10^{24}	28901	988	840668
50%	1.95×10^{23}	2.56×10^{21}	1.67×10^{24}	102269	1341	872533
60%	3.67×10^{23}	3.39×10^{21}	1.74×10^{24}	191921	1772	911588

70%	5.88×10^{23}	4.45×10^{21}	1.84×10^{24}	307520	2329	961958
80%	8.99×10^{23}	5.95×10^{21}	1.97×10^{24}	470485	3115	1033133
90%	1.43×10^{24}	8.53×10^{21}	2.21×10^{24}	749126	4461	1155225

* Values only represent decrease from initial reaction rate and not increases in rates from transmutation or breeding.

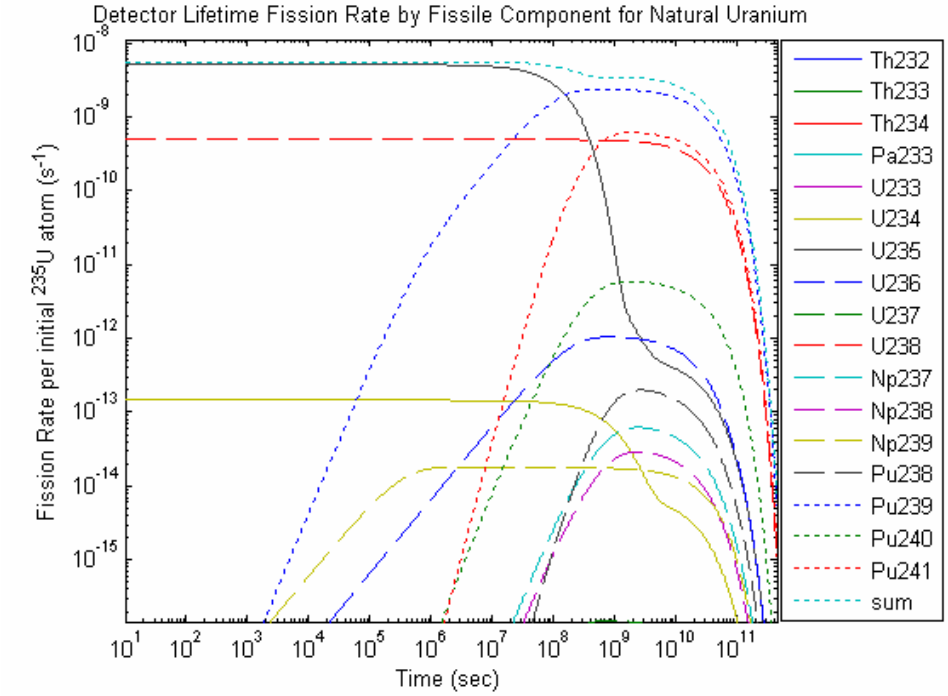

Figure 12: Detector lifetime fission rate by fissile component for natural uranium.

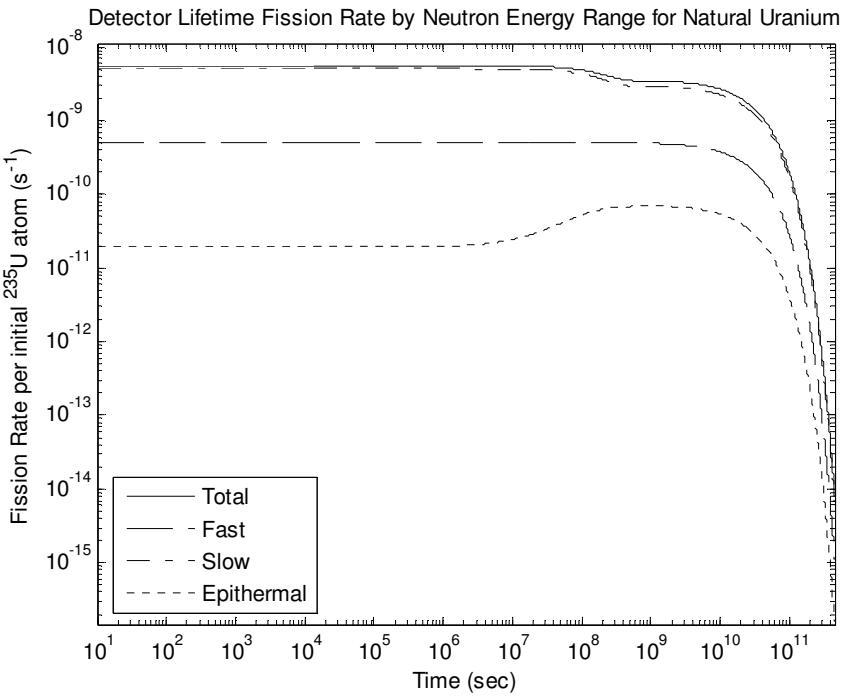

Figure 13: Detector lifetime fission rate by neutron energy range for natural uranium.

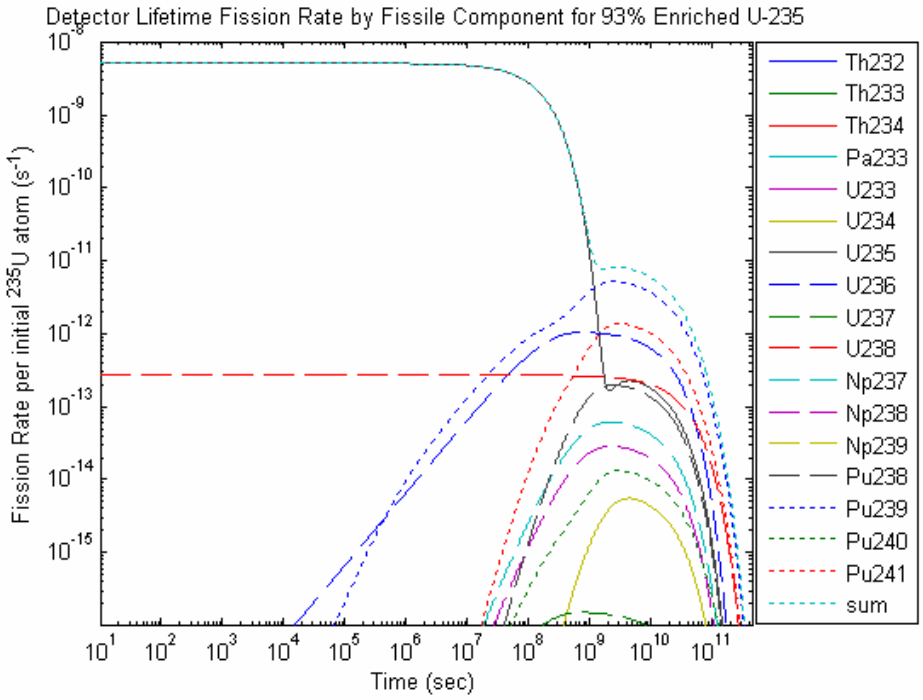

Figure 14: Detector lifetime fission rate by fissile component for 93% enriched ^{235}U.

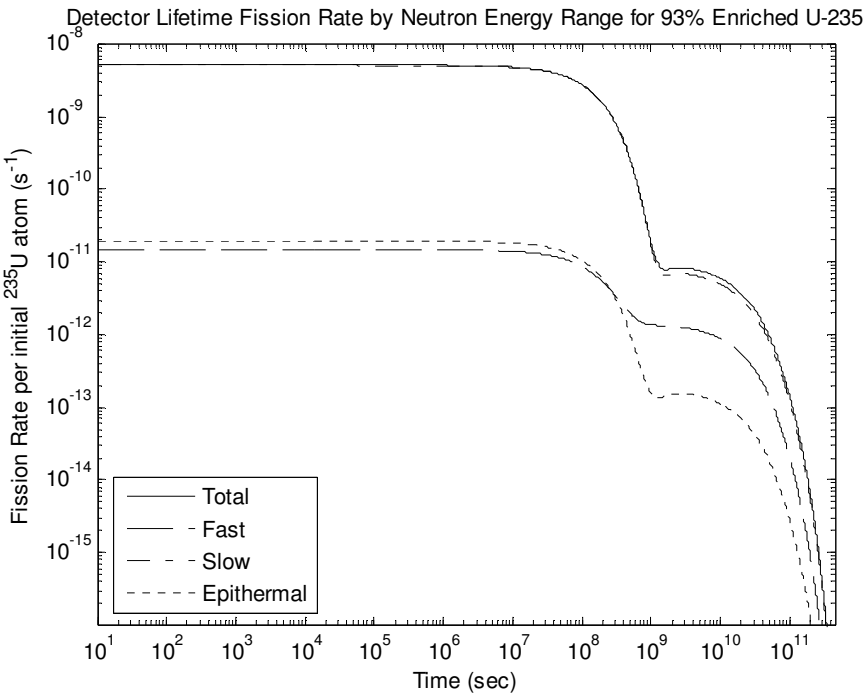

Figure 15: Detector lifetime fission rate by neutron energy range for 93% enriched ^{235}U.

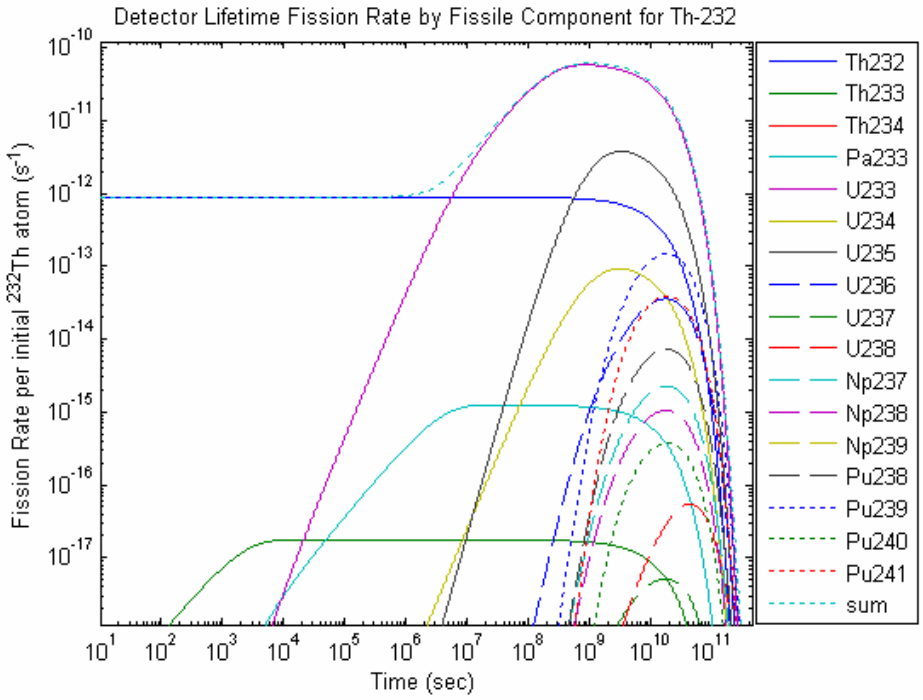

Figure 16: Detector lifetime fission rate by fissile component for ^{232}Th.

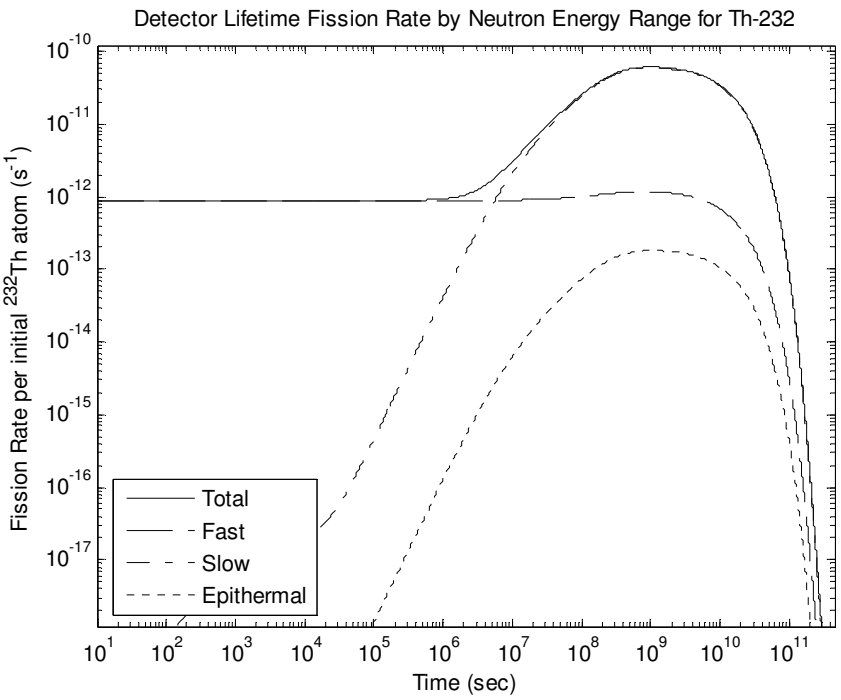

Figure 17: Detector lifetime fission rate by neutron energy range for ^{232}Th.

Lifetime Optimization.

Optimization of the detector lifetime may be accomplished through the use combinations of different reactive material coatings. While there is nearly a limitless number of coating combinations available through mixtures of fissile, fissionable, and fertile materials, this optimization example is limited to only various enrichments of uranium mixed with thorium. Enrichment of ^{235}U will control the concentrations of ^{234}U, ^{236}U, and ^{238}U per the data in Table 7 and since Th-232 is the only isotope present in natural thorium, there are only two parameters to vary for optimization, uranium enrichment and uranium to thorium ratio. In this optimization we are not only concerned with lifetime longevity as in the previous section, but also in the flatness of the detector response over time.

Table 7: Isotope concentrations in U.S. DOE uranium (wt% [at%]) [31].

^{235}U		^{234}U		^{236}U		^{238}U	
93	[93.06]	1.0	[1.005]	0.445	[0.4434]	5.555	[5.489]
50	[50.03]	0.425	[0.427]	0.231	[0.2302]	49.344	[48.75]
4	[4.003]	0.0334	[0.0336]	0.0154	[0.01535]	95.9512	[94.80]
0.9	[0.9006]	0.00948	[0.00953]	0.00325	[0.00324]	99.08727	[97.90]
0.711 (natural)	[0.7115]	0.00541	[0.00544]	0.00	[0.00]	99.28359	[98.10]
0.2 (depleted)	[0.2001]	0.00356	[0.00358]	0.00	[0.00]	99.79644	[98.60]

A simplified set of optimization conditions are used in order to find the optimized solution without a large computational overhead. The optimization program begins by setting up

an initial matrix of enrichment and ratio parameters. This matrix is initialized by user defined upper and lower limits for both parameters with a user defined number of steps within these limits. The user also specifies a maximum percent signal change which defines a flatness band. For example, a 1% maximum signal change defines a band of ±1% of the original detector fission rate, or response, which the detector response must stay between. When each enrichment and ratio combination is used to calculate the lifetime response, the optimization program stores to time at which the detector response breaks this band and whether the response is increasing or decreasing at that time. These two pieces of data are used to define a new matrix of parameters for further analysis. The new matrices are defined by examining analyzed parameter values around the parameter which yielded the longest lifetime and the parameter in which the response slope changes direction. These new matrices are then analyzed and the process is repeated until the optimized enrichment and ratio values are determined to within 0.000001.

Two cases of reactor operations have been optimized. The first is for full power continuous operation as used in the analysis of Section 0. However, the Kansas State University TRIGA Reactor does not operate at full power and does not operate continuously. While the programs utilized cannot account for different periods of operation and shutdowns, an averaged power may be used. The first quarter of 2005 produced 33,447 kWh of power. Using this value the projected total power for year 2005 is 133,788 kWh [32,33]. Continuous operation at full power will yield 2,190,000 kWh. Therefore an average power for continuous operation is 15.273 kW. Optimized enriched uranium and mixtures of enriched uranium and thorium are presented for both operation cases in Table 8. One should notice the significant lifetime increase obtained through this optimization method. Plots showing the lifetime response are shown in Figures 18.0 through 21.0 .

Table 8: Optimized neutron reactive mixtures and lifetimes in years for full power and average power (15.273 kW) continuous operations (calculations based on 1% signal change optimization).

Mixture	Signal Change 1% (years)		5% (years)		25% (years)	
	full power	***average power***	***full power***	***average power***	***full power***	***average power***
0.51701 wt% ^{235}U	2.867		4.817		162.5	
0.52089 wt% ^{235}U		44.12		72.75		358.6
60% - 1.1843 wt% ^{235}U 40% - ^{232}Th	58.58		89.49		244.3	
45% - 1.7826 wt% ^{235}U 55% - ^{232}Th		842.5		1310		3513
Natural Uranium (0.711 wt% ^{235}U)	0.2581	5.163	1.348	22.53	6.882	107.0
Highly Enriched Uranium (93.0 wt% ^{235}U)	0.02867	0.4694	0.2581	4.224	1.520	24.88
^{232}Th	*	*	0.0287	*	0.0573	*

* Value was less than resolution of lifetime optimization program - 3.171×10^{-8} years or 1 second

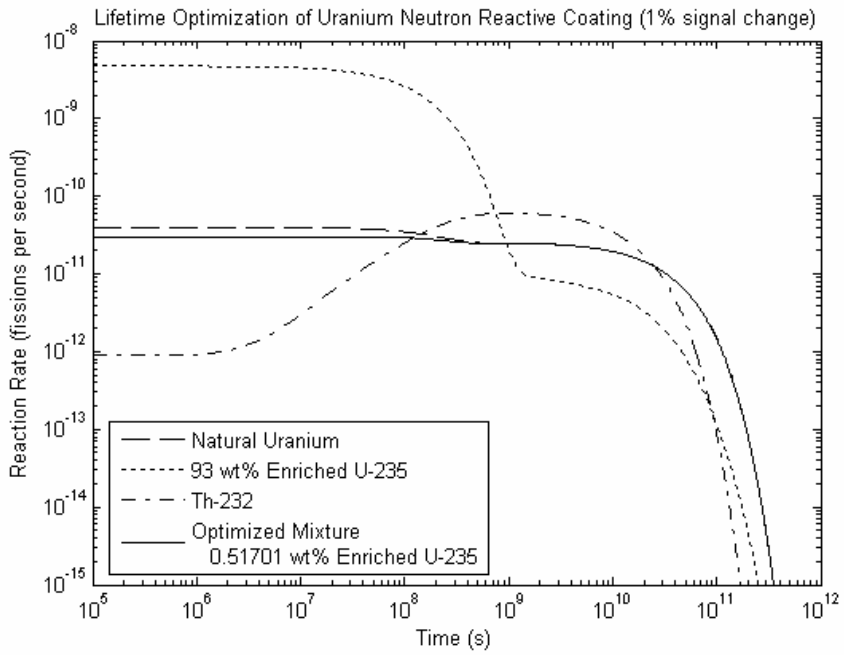

Figure 18: Lifetime optimization using enriched uranium for full power continuous operations.

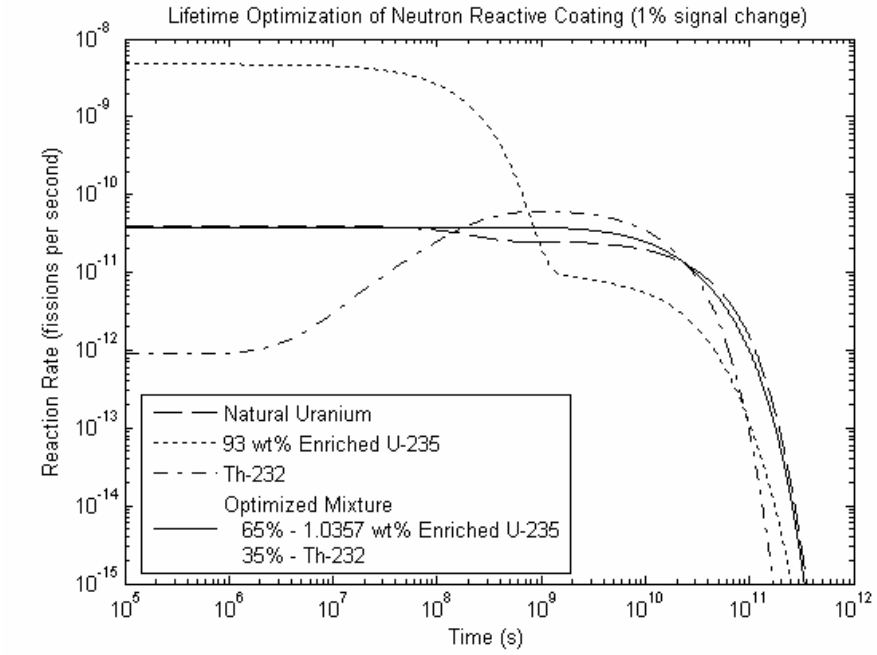

Figure 19: Lifetime optimization using a mixture of enriched uranium and thorium for full power continuous operations.

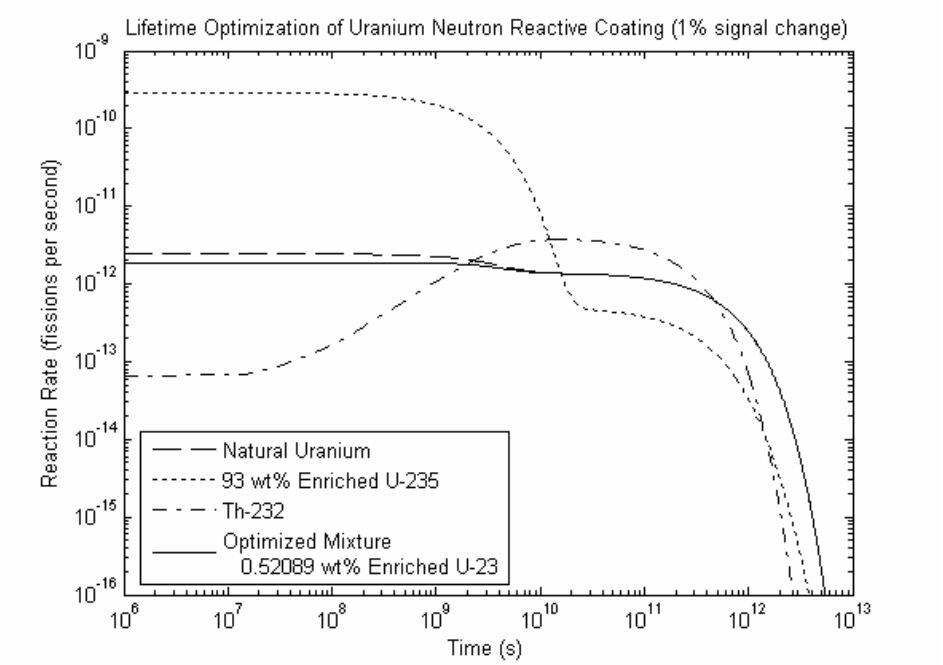

Figure 20: Lifetime optimization using enriched uranium for 15.273 kW continuous operations.

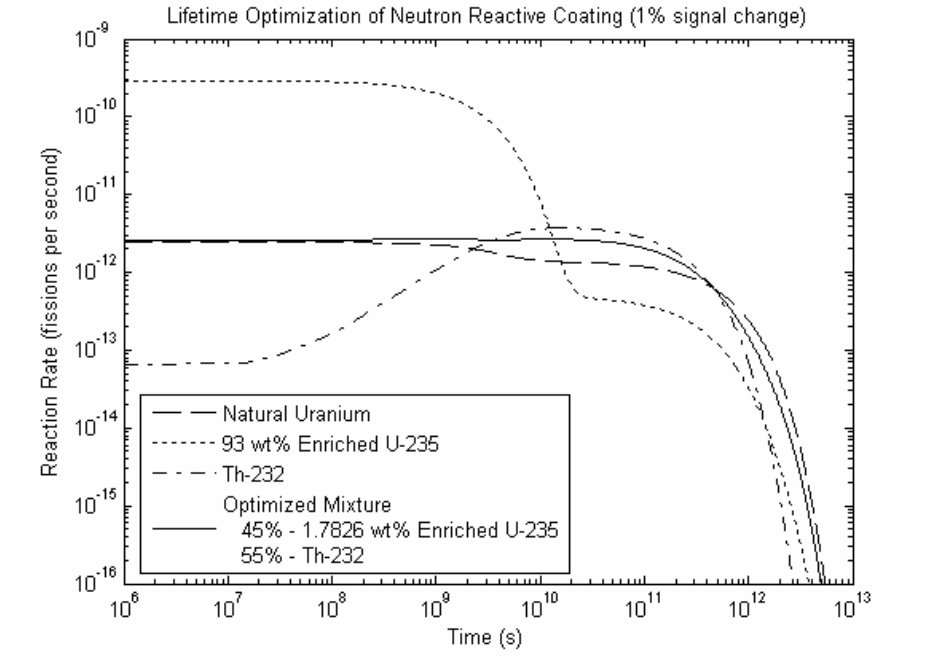

Figure 21: Lifetime optimization using a mixture of enriched uranium and thorium for 15.273 kW continuous operations.

PROTOTYPE CONSTRUCTION AND TESTING

Many varieties of MPFD prototypes were designed, built, and tested. The lessons learned from these prototypes are used to shape the design guidelines for the finalized MPFD design. This chapter discusses the designs and construction methods of 4 major sections: the substrates, the electrically conductive contacts, the neutron reactive coatings, and the methods of sealing the detectors.

Substrates

Substrate material for the MPFD can be any kind of insulative which can be sealed to hold a fill gas. Green Tape™ from DuPont is a green, or unsintered, ceramic and was one of the first products to be tried as a substrate. The product was selected because it comes as a flexible and easily formed thin strip [34,35]. The Green Tape™ can be formed into different shapes with simple tools such as a razor blade or biopsy punch. Multiple layers can be hermetically sealed together along with embedded conductive traces, vias, and electronic components such as resistors and capacitors. Because of these features, Green Tape™ is used throughout industry for the manufacture of circuit boards and substrates, which is an inexpensive technology for industrial use. Additionally, the main constituent of Green Tape™ is alumina, which has a low neutron absorption cross section thereby being relatively neutron transparent.

Hermetic sealing of multiple layers of unsintered Green Tape™ is possible through the use at 3000 psi press heated to 70ºC. The sintering process requires a furnace capable of reaching 800ºC. As the Green Tape™ is sintered, the substrate undergoes shrinkage. With even heating, this shrinkage is predictable and can even be used as an advantage by designing the substrate to shrink around wires and form permanent seals. However, the downside of this shrinkage is that the embedded conductive traces, vias, and electronic components must shrink at the same rates as the Green Tape™. Such conductors are available, but contain either gold or silver. Gold will activate and decay into mercury which could attack aluminum parts such as the housing of the detector string or other reactor components. The most significant disadvantage is cobalt in the Green Tape™, apparently added to produce a bluish-green tint. This is problematic, at least for research, since cobalt has a large neutron cross section for activation and a long half-life, which quickly makes irradiated detectors nearly impossible to handle in the short term.

Some of the problems with Green Tape™ were thought to be resolved with a closely related product, Mistler, Inc.'s Alumina Tape Ceramic. This product is also a green, or unfired, ceramic material but is made from alumina with a small amount of MgO. When fired it is nearly identical in all properties as an alumina substrate. Unlike the Green Tape™, the alumina tape does not need pressure and heat to form a hermetic seal, instead it only takes a light misting of isopropanol. Once misted the unfired pieces may be placed on top of each other and when dried they cannot be separated. Light pressure applied by a roller helps remove any air trapped between the substrates. The disadvantages of the alumina tape become apparent during the firing, or sintering, process. The main problem is the sintering temperature requirement of 1650°C which requires a special very high temperature furnace. In addition, it is recommended to use a weight on top of the alumina tape during sintering to help keep the edges from curling. The temperature changes must also be carefully controlled to keep the shrinkage constant and to keep the substrates from cracking due to thermal strain. Unfortunately Kansas State University did not have the furnace or equipment needed to sinter the substrates.

Figure 1 shows two Alumina Tape Ceramic substrates. All of the holes and outer shape were cut freehand using a set of biopsy punches and a razor blade. The bottom substrate was assembled from two substrate pieces which were laminated together using the previously discussed procedures. The substrates were sent to Honeywell for sintering. The gold contacts were then applied by physical vapor deposition (PVD) with the shapes defined by a simple kapton tape mask. While this technology has proved viable for making the detector substrates, development of the Alumina Tape Ceramic substrates was suspended due to the concern of mass production of identical substrates through the S.M.A.R.T. Laboratory.

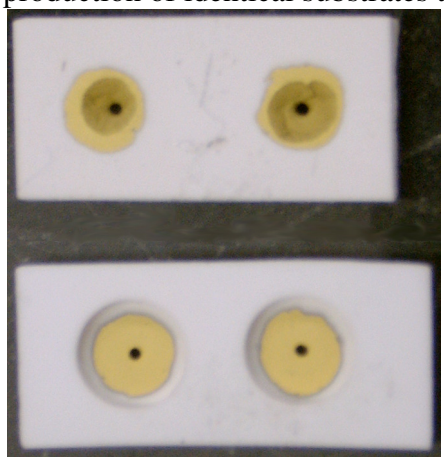

Figure 1: Prototype detector made from Alumina Tape Ceramics.

In order to complete the goals of the project in a timely manner it was decided to use manufactured alumina substrates instead. Alumina (Al_2O_3) properties are well known and it is utilized for its radiation hardness and ability to withstand extreme temperatures. It is also a commonly available material, but due to its hardness after sintering it must be machined using specialized tooling. Overall it was determined that Al_2O_3 would be best suited for the development of the MPFDs.

Electrically Conductive Contacts

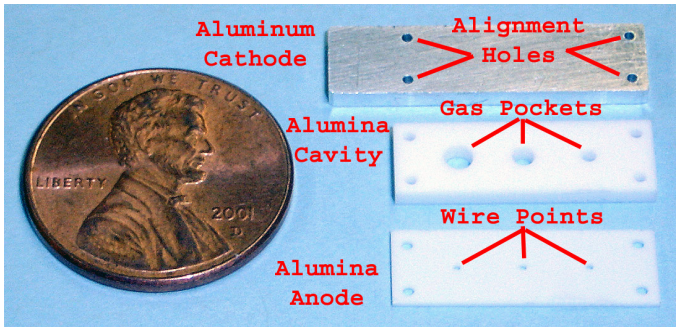

Figure 2: Manufactured 3-chamber alumina substrates and aluminum backing plate.

One of the first substrates designed specifically for prototyping the MPFDs included cavities for detector arrays with three chambers of different sizes (Figure 2). The detector array

could either be formed entirely from alumina, or an aluminum backing plate could be used as a common cathode for all three chambers. The alumina backing substrate had three identical holes, or wire points, located in the center of the chambers for the addition of a wire to form the anode connections. With the wires held in place by an epoxy, all of the substrate pieces are assembled together with the same epoxy. The alignment holes in all of the substrates allow a pined jig to hold all of the substrates together during the epoxy curing process. This assembly exposed two significant problems with the contact design. The first problem was encountered when trying to form a good seal around the wires. Temperature fluctuations would cause the substrate, epoxy, and wire to shrink or expand at different rates and thus gaps would form and cause the seal to be broken. The other potential problem was the surface smoothness of the contact. The penetrating wire would be cut off as close to the contact surface as possible using a razor blade, however, a small bump would often be left over which would cause a disturbance in the detector's electric field. Depending on the roughness and the height of this bump, the electric field could be affected enough to change the response from detector to detector.

Another detector design used a set of substrates shown in Figure 3. Two of these substrates had a contact pattern evaporated on one surface, which formed the cathode and anode pieces, while the other substrate had a central hole which was used to form the center cavity or pocket. Once fused together, a wire was inserted into one of the alignment holes which had a contact running to it. A conductive epoxy filled the hole and tried to make a connection between the contact and the wire. This method was successful as it did produce the very first MPFD, but was not reliable since the only connection to the contact was only through the cross section of the contact along the edge of the alignment hole.

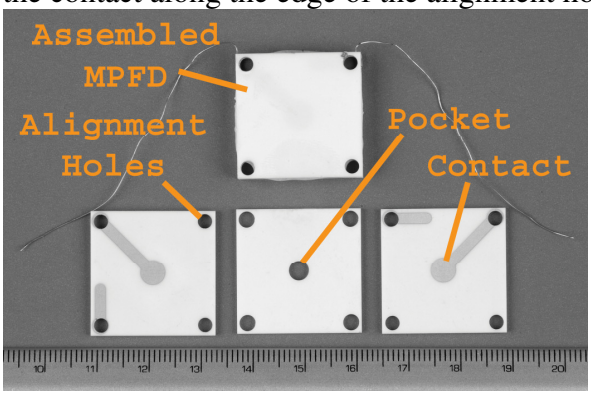

Figure 3: Using spare alumina substrates to form an MPFD. Shown is actually the very first prototype MPFD ever built.

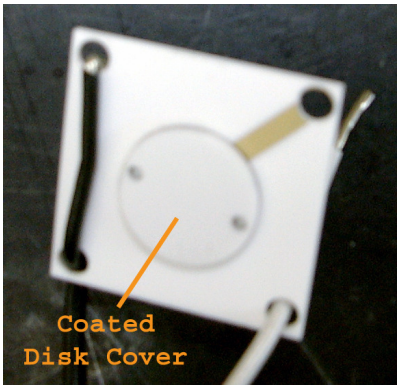

Figure 4: A different design trying to get good contact between the anode and cathode and their respective wires.

A variation on the square substrate design was utilized in order to try and get a better electrical connection to the anode and cathode contacts while maintaining a flat surface inside the chamber. The square substrate of Figure 4 was the substrate containing the pocket but was coated on both sides with the contact pattern of the other square substrates of Figure 3. The anode and cathode are provided by a smaller disk which had one side entirely coated with gold. This design allowed the wires to be epoxied directly onto the contact surface thus providing a better electrical connection than just relying on the contact cross sectional area through the hole. However, the connection between the coated disk cover and the contact proved unreliable. The resistance of the connection varied widely as the two surfaces would often get covered by epoxy while sealing the disk to the square substrate.

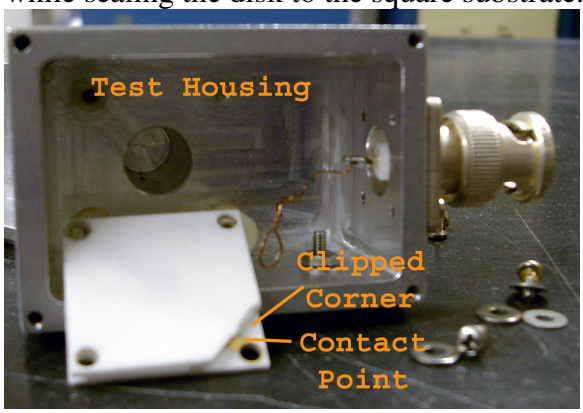

Figure 5: A successful and reproducible contact design ready for beam port testing.

These trials led to a successful and reproducible construction method which utilized characteristics of both of the previous square substrate designs. Figure 5 shows the return of three square substrates as assembled in Figure 3, but the contact surface has been exposed by cutting away the corners of the other two substrates. By removing the corners it was then possible to make a good connection to the contact surface while having a continuous conductor from the wire and into the chamber. This feature was determined to be essential for the mass production of reliable detectors and its design has been incorporated into the final generation of substrates as discussed in Section 0.

Neutron Reactive Coatings

Application of the neutron reactive coatings to the detectors can be done through a variety of methods. The first MPFD built used a boron coating deposited with physical vapor deposition (PVD) with the S.M.A.R.T. Lab's electron beam evaporator. While PVD would most likely be the ideal method of applying neutron reactive coatings for the mass production of MPFDs, contamination with radioactive materials in our systems is not an option. Further, we would have to receive Kansas State University Environmental Health and Safety approval to run such an operation when using combinations of natural uranium, highly enriched uranium, and thorium. Hence, other methods for depositing the material were investigated. It was learned that simple coatings could be deposited by drying a drop of uranyl nitrate and deionized water solution [36]. An Eppendorf pipette was used to deposit the desired volume of solution onto the contact area inside the pocket, followed by baking the substrate with an infrared heat lamp. The surface tension of the solution often caused the solution to only cover a small portion of the cavity area, hence a small paint brush was used to spread the solution across the full cavity area. However, the method did not allow for the repeatable or reliable fill thicknesses. Other methods of spreading the solution, such as rocking the substrate while drying, were attempted, but a uniform coating thickness was elusive.

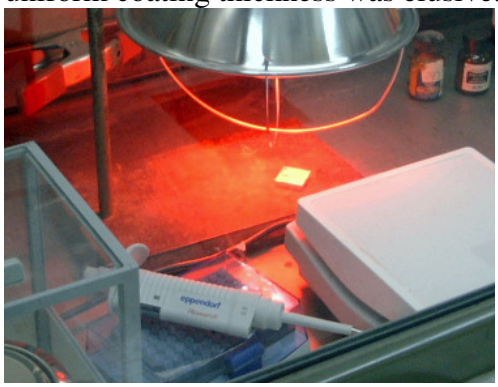

Figure 6: A uranyl nitrate drop is deposited on a substrate surface and dried under an infrared heat lamp.

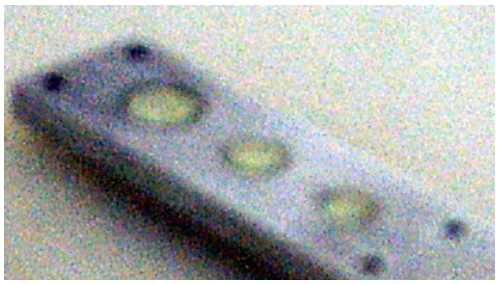

Figure 7: The dried neutron reactive coatings.

Electrolysis, or electroplating, allows for control of the coating thickness, and can in fact be used to deposit uniform coatings. To achieve consistency on all of the detectors, a specialized system was constructed (details on this system are reserved for Section 0).

Sealing the Detectors

While the use of unsintered substrates allowed many methods of hermetically sealing detector components prior to sintering, the use of machined alumina substrates does not. Straight forward methods available to seal the pieces are with a bonding epoxy between substrate pieces, or entirely encapsulate the detector in an epoxy.

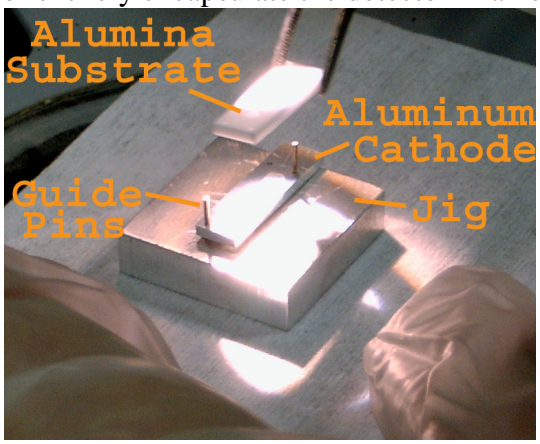

Figure 8: Manufactured 3-chamber alumina substrates and aluminum backing plate being assembled using a guide pin jig.

Figure 8 shows the assembly of two substrates from Figure 2 using guide pins that go through each layer of the substrates. These pins make sure the substrates stay aligned during the epoxy curing process. With the small sizes of the detectors, the use of some kind of alignment device is critical in being able to position the substrates correctly.
However, the use of pins sometimes destroyed detector since any small excess epoxy would glue the pins inside the holes. When trying to remove the detector from the jig, the substrates would often break before the pin could be removed. Therefore, a different method of alignment needs to be developed for use during assembly.

DESIGN CONSTRAINTS

The primary purpose of the MPFD project is to deploy an array of neutron detectors throughout the Kansas State University TRIGA Mark-II Nuclear Reactor for neutron flux monitoring. While this thesis does not cover the full deployment of the detectors, the design of the MPFDs is constrained by this goal. When appropriate, the design constraints were expanded to allow the MPFDs built for the Kansas State University TRIGA Reactor to be capable of operating in power reactors without major design modifications. These power reactor designs considered are pressurized water reactors (PWR), boiling water reactors (BWR), naval reactors, advanced CANDU reactors (ACR), and advanced concept reactors commonly known as Gen IV reactors.

Design limitations imparted by various reactor designs are presented in the following chapter. These limitations include the size constraints, radiation hardness, radiation monitoring, and overall cost.

Deployment in the Kansas State University TRIGA Mark-II Nuclear Reactor

Deploying MPFDs in the Kansas State University TRIGA Reactor imposes several restrictions on their design. The major constraint is on the size of the detector package, mainly due to the limited locations where the MPFDs may be deployed inside of the core. Other constraints are based on the high radiation fields found in the reactor core which significantly limits the materials which may be used. There are also thermal considerations for the detector materials, although forgiving to a large degree in the Kansas State University TRIGA Reactor.

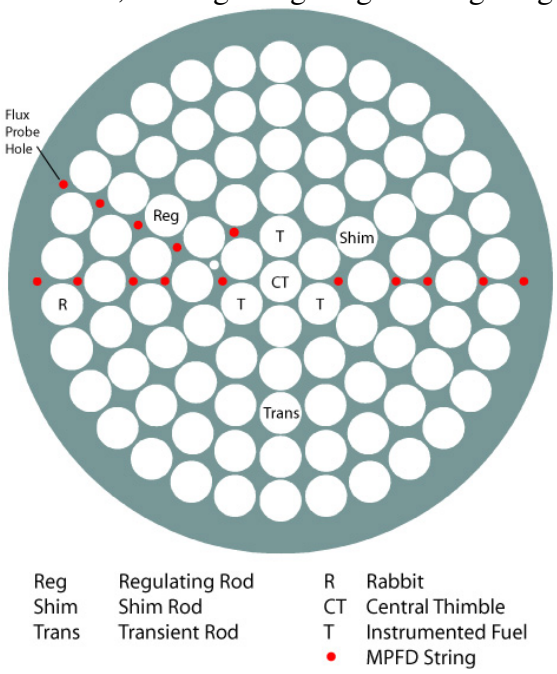

Figure 1: Existing Kansas State University TRIGA Reactor core configuration II-21.

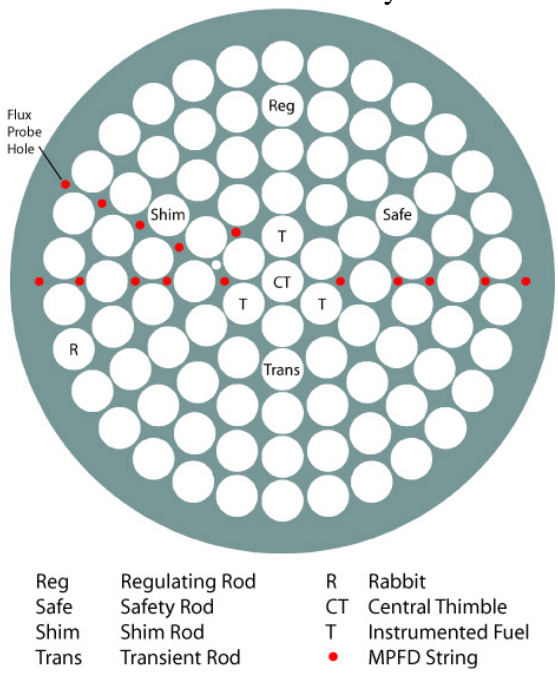

Figure 2: Future power upgrade core configuration III-1 with the addition of a fourth control rod.

Dimensions

There are two primary core dimensions of interest for setting the design constraints of the MPFDs. The first is defined by the locations where the detectors will be deployed. Figures 1.0 and 2.0 show the existing core configuration and the future upgraded core configuration of the Kansas State University TRIGA Reactor, respectively. A series of 15 small flux probe holes have been highlighted in red to show where MPFD strings will be located inside the core. These holes already exist in the upper and lower grid plates and are 8 mm (0.315 in) and 4 mm (0.157 in) diameter, respectively. These hole dimensions have determined the sizing constraints of the detectors and housing. The hole dimensions have also affected the number of detectors in each string assembly due to a limited number of readout and voltage wires that will fit inside the housing.

The spacing between detectors is determined using the second dimension of interest, the length of the fuel. Each fuel element is 72.1 cm (28.37 in) long and 3.37 cm (1.47 in) in diameter. However, the fuel element has 8.74 cm (3.44 in) graphite reflectors at both ends of the element. The actual fuel, or meat, of the element is only 38.1 cm (15 in) long as shown in Figure 3 [29,37]. The maximum number of wires that can fit in the tube and the number of

measurements required for back projection calculations determined that only five sets of MPFD^3-T needs be in each string assembly.

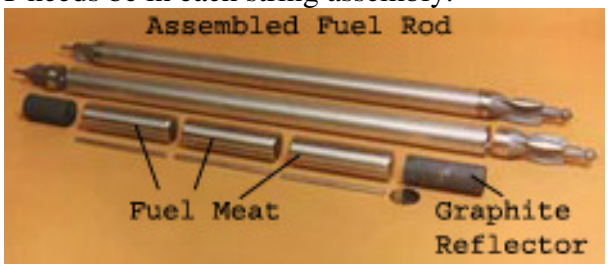

Figure 3: Parts of a fuel rod used in the Kansas State University TRIGA Mark-II Nuclear Reactor [37].

A secondary constraint for the full MPFD assembly is the spacing requirements to carry out fuel inspections. A minimum vertical spacing of one fuel element length plus the spacing needed to attach and maneuver the fuel handling tool is needed for these operations. A vertical clearance of approximately 107 to 122 cm (3.5 to 4 feet) is needed for such operations. Otherwise, the MPFD assembly would have to be removed in order to perform the fuel inspections.

Additional dimensions that affect other system components are the physical tank and the location of the reactor core inside the tank. The tank is 1.98 m (6.5 ft) in diameter and is 6.25 m (20.5 ft) deep. The core is 4.88 m (16 ft) below the water surface and is located in the center of the tank [29]. A cross sectional view of the reactor tank is shown in Figure 4.

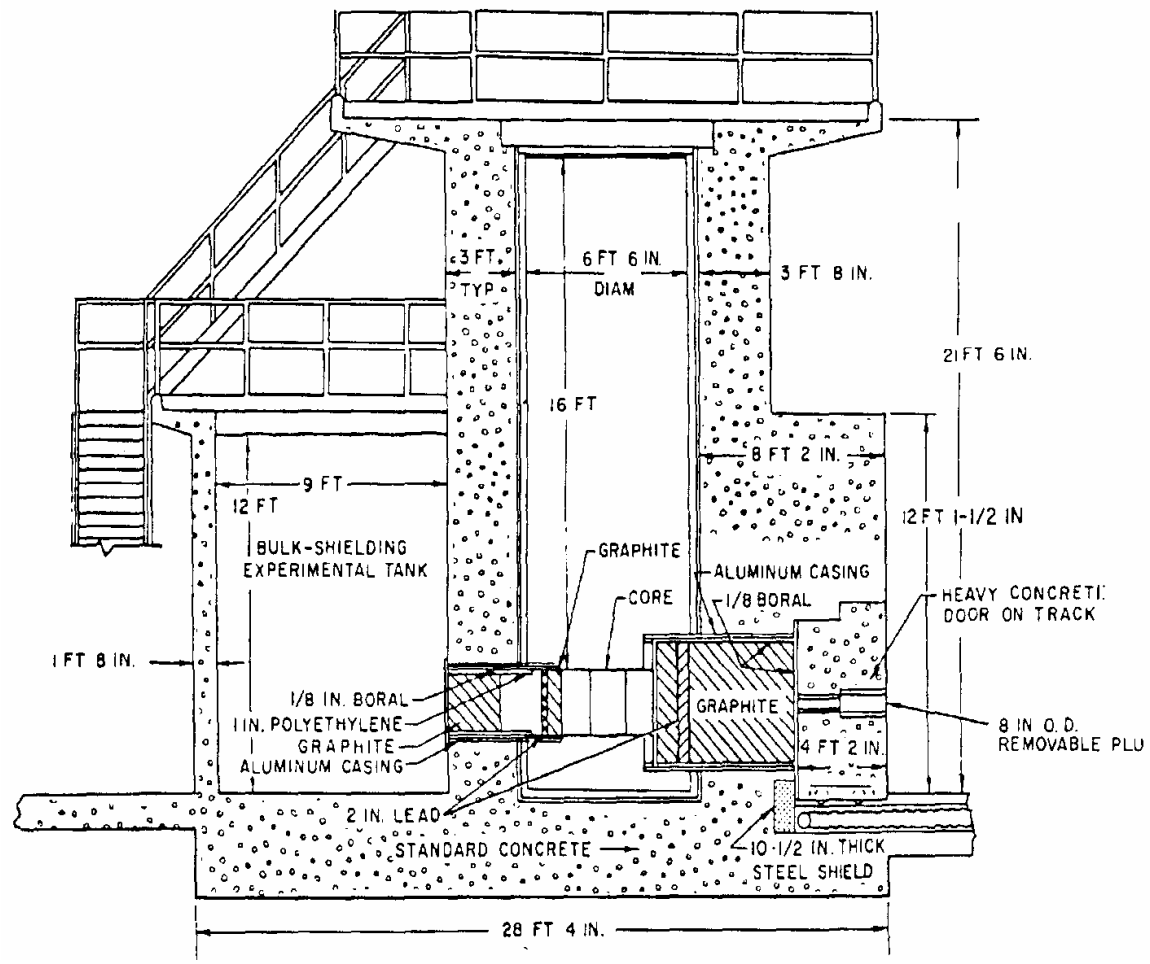

Figure 4: Vertical cross section of the Kansas State University TRIGA Mark-II Reactor [29].

Radiation Doses

The highest radiation doses are found in the center of the reactor (or in the central thimble). Experimental measurements for the existing core configuration (Figure 1) at full power (250 kW) indicate the fast neutron flux is 1.2×10^{13} n cm^{-2} s^{-1}, the slow neutron flux is 1.0×10^{13} n cm^{-2} s^{-1}, and the gamma-ray dose rate is 2.5×10^{4} rad s^{-1} [29]. It can be assumed that the neutron flux and gamma-ray dose rate will increase linearly with the future power upgrade to 1.25 MW, thus increasing them by a factor of five. Neutron fluxes and gamma-ray dose rates of this high magnitude impose special design limitations to be considered when selecting detector materials. The substrates, electrical contacts, fill gas, epoxies, wiring and housing must all be made of materials which can withstand the high radiation fields.

Temperature

The Kansas State University TRIGA Reactor license limits the maximum primary water temperature to 48.9°C (120°F) and the maximum fuel temperature to 450°C (842°F) [29]. While the detectors will be inserted between fuel elements, they will be housed in water tight tubes surrounded by the primary water. Even so, the primary water temperature is for the bulk tank

and thus the water temperature directly in the core can be significantly higher than the 48.9°C limit.

Number of MPFDs

A secondary purpose of this project is to unfold the power density of the fuel using data from the full in-core deployment of detectors, hence it is necessary to deploy as many detectors as possible throughout the core. From the discussion in Section 0, there are only five MPFD^3-T per string and a total of fifteen strings is to be inserted in the core (Figures 1.0 and 2.0). Therefore the total array will consist of 75 MPFD^3-T, each having 3 detectors (fast, slow and background) for a total of 225 detectors. Such a large number of detectors requires specialized electronics and data collection programs in order to gather data from all of the detectors simultaneously.

Additional Environmental Monitoring

Besides the neutron and gamma-ray fluxes, temperature will also have an impact on the performance of the detectors. The changing temperature will cause the fill gas to change pressure according to $PV = nRT$ or $\frac{P_1}{T_1} = \frac{P_2}{T_2}$ since the volume is held constant. As explained in Section 0, the change in pressure will cause a change in the drift velocity of the ions and electrons of the ionized fill gas. The temperature will also affect the resistivity of the contacts and wires. While these changes in drift velocity and resistivity are just a few of the temperature affects on the detectors, they alone show that, at least for research purposes, the temperature at the detector needs to be monitored.

Detector Shielding and Wiring

In order to reduce electromagnetic (EM) noise interference, the detectors will be housed inside a metal tube for shielding. While a very low resistivity metal, such as copper, is preferred for EM shielding, the high radiation fields and deionized water environment requires low activation and low corrosion materials, such as aluminum. At distances of approximately five feet from the core the neutron flux is decreased by eight orders of magnitude and thus a higher strength material, such as stainless steel, may be used to improve structural support.

The spacing between wires, the distribution of signal and DC wires, and the straightness or twisting of the wires all have a major impact on the noise and crosstalk between the wires [38]. Insulation must be provided in order to electrically isolate the wires from each other. The radiation doses will be extremely high in and around the reactor core, hence typical plastic insulation will quickly degrade and fail requiring an alternative insulation scheme.

Neutron Reactive Coatings

It is critical that the different neutron reactive coatings do not mix when applying them to the detector. For example, the MPFD^3-T has three different detectors, those being fast, slow, and background, in one package. While the background detector will have no coating, the fast and slow detectors require different coatings. If using PVD or sputtering technologies for depositing the coatings, a simple shadow mask should provide the necessary isolation. However, when using electroplating techniques, the substrate is usually immersed in the plating solution, which requires a different method of separating the exposed sections.

Cost

A secondary goal of this project is to produce an inexpensive technology that can be commercialized. Present day commercial fission chambers typically cost thousands of dollars, mainly due to materials and labor cost associated with their manufacture. One method of reducing cost is to use inexpensive, readily available materials, while also reducing the quantity of the materials needed.

Expanded Constraints

Additional value will be added to the project if the resulting devices are capable of surviving conditions within other reactors. Some of the most extreme reactor conditions will be within some of the proposed Gen IV reactors. Some Gen IV reactors have proposed temperatures ranging up to 1000°C (1832°F) (VHTR) with pressures reaching 25 MPa (246.7 atm) (SCWR) [39]. While most thermal light water reactors (LWR) in operation today utilize fuel through a 4½ to 6 year cycle, rotating out a third of the core every 1½ to 2 years, the proposed LFR will have a core life of 10 to 30 years, and current U.S. Naval reactors are designed with a core life between 30 to 50 years [39]. Some reactors operate utilizing slow neutrons while others are designed to operate using a fast neutron spectrum. The neutron fluxes of these reactors vary from 10^{12} to 10^{15} n cm^{-2} s^{-1} with an average of 10^{14} n cm^{-2} s^{-1} for LWRs in the United States.

DESIGN SOLUTION

The final substrate design was developed through the experience gained from the construction of multiple prototypes and the requirements set by the design constraints.

Substrate Design

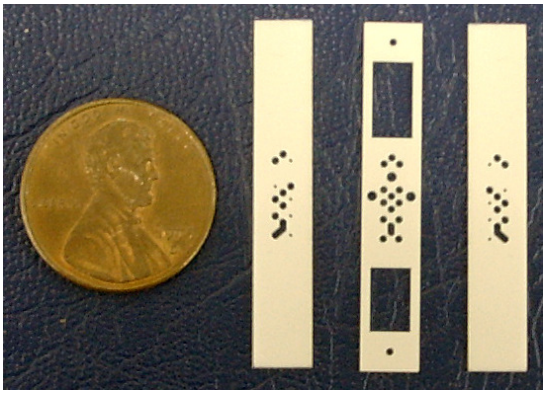

Figure 1: MPFD^3-T alumina substrates.

Two versions of 96% alumina ceramic based substrates make up the MPFD^3-T configuration as shown in Figure 1. One of the versions defines the center substrate (cavity) while the other version forms both outer substrates (base). It is upon these base substrates that the electrodes are deposited for the electrical connections to three detectors and a thermal sensor. Two large gas storage chambers are built into the cavity substrate along with gas flow channels which link the detector chambers together (see Figures 2.0 and 3.0). Additional special holes are present in both the cavity and base substrates for securing and routing wires while ensuring good

electrical connections. All of these features are built into a combined package of 34.3 mm (1.35 in) long by 5.7 mm (0.225 in) wide and 1.5 mm (0.060 in) thick. The next several sections of this chapter describe the features in detail.

Gas Fill/Flow Solution

One possible method of filling an MPFD gas pocket with the desired fill gas is to seal the three detector substrates (cavity and two bases) inside a glove box containing the fill gas atmosphere. The fill gas will then be trapped in the chambers once the epoxy has cured and sealed the detector. However, most epoxies will outgas as they cure which will contaminate the fill gas. This contamination will change the performance of each detector and will shorten the detector life. The second method of filling the gas pockets is to seal the detector with the exception of a small fill channel. Once the epoxy has been cured, the gas pocket is evacuated and then backfilled through the fill channel. A small plug of epoxy then seals the fill channel. This plug introduces a much smaller amount of contamination thus keeping the fill gas as pure as possible.

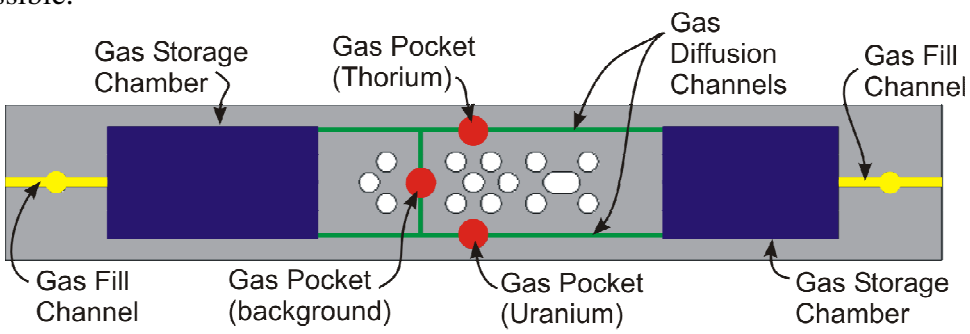

Figure 2: The cavity substrate of the MPFD^3-T shown with gas fill/flow features highlighted.

The MPFD^3-T is designed using the second method of adding fill gas in order to keep the fill gas pure. The cavity substrate (Figure 2) has two of these small fill channels (yellow) on either end of the substrate. This allows faster and more efficient flow during evacuation and backfilling than a single channel. In addition, if one of the channels becomes blocked the detector can still be utilized through the use of the second channel. A round bulge is present in the center of each gas fill channel which allows the epoxy plug to wedge into the bulge and reduce the potential of plug failure.

The gas fill channels are connected to two large gas storage chambers. These chambers (blue) are then connected to each gas pocket (red) through gas diffusion channels (green). Each gas pocket, which makes up the actual detector chamber, is entered by two diffusion channels from opposite sides. Similar to the gas fill channels, this duplication allows blockage of one path without causing failure of the detector while also increasing the evacuation and backfill ability of the chambers. By increasing the available high purity fill gas volume through the large gas storage chambers the overall purity of the fill gas in the gas pockets may be kept high. Contaminates will develop inside the gas pockets due to buildup of gaseous fission products of the neutron reactive materials. These contaminates will diffuse through the gas diffusion channels and into the gas storage chambers, thus reducing the contaminant level in the gas pockets. Maintaining the high gas purity through contaminant diffusion and through limited epoxy out gassing will help to extend the detector life and maintain consistent performance.

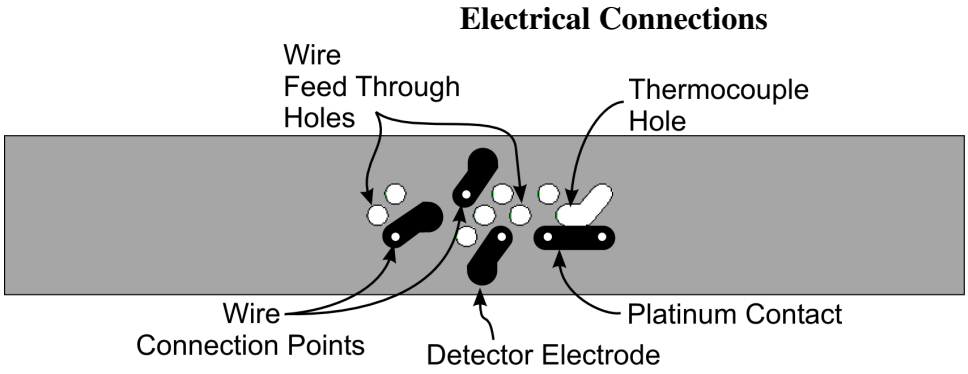

Figure 3: The base substrate of the MPFD^3-T shown with electrical coatings.

Through the construction and testing of multiple prototype MPFDs, it was found that reliable electrical connections are an important design feature of a good MPFD, resulting in the present design shown in Figure 3. Platinum contacts are applied to the base substrates in four patterns. Three of these patterns define a continuous link between the detector chamber electrode and the wire connection point. The fourth pattern is used for connection between a wire connection point and a thermal monitor (thermocouple), described further in Section 0. The base and cavity substrate is designed to form a pocket around the wire connection points after the substrates are stacked, as shown with the semi-transparent overlay of the detector substrates in Figure 4. A wire is inserted into the pocket through the smaller hole (wire connection point) in the back of the substrate, and conductive epoxy is filled around the excess wire sticking through the pocket so as to make electrical connection. This also provides a mechanical bond between the epoxy and wire which provides mechanical strength.

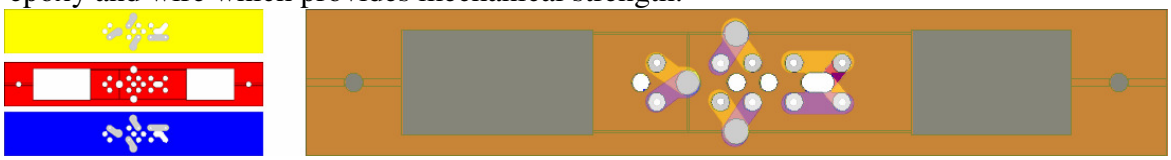

Figure 4: Semi-transparent overlay of the two base substrates with platinum electrodes and the cavity substrate showing how the different components work together.

The orientation and placement of the detector chambers were mainly determined by the electrical connections and the distribution of the wires. In order to ensure isolation between the wires and the detector housing, the wire connections were located towards the center of the substrates. Distributing the wires from the center to the outside also allows a greater number to be packed around the detectors.

Additional holes are provided down the center of the substrate as wire feed through holes. The hole placement allows wires connected on one side of the substrate to be routed through the substrate sandwich and placed on the opposite side of the substrate. Commercially available alumina tubes are used in bundles to separate the wires.

Embedded Environmental Monitoring

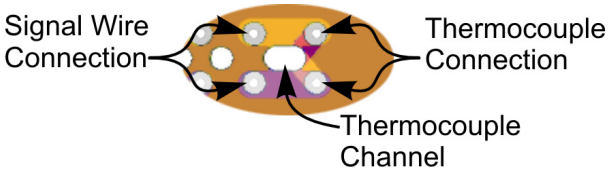

Figure 5: Expanded view from Figure 4 showing the embedded thermocouple location.

In order to assist in determining the temperature dependence of the detectors, the MPFD^3-T is capable of being equipped with a two wire environmental monitor. The design of the monitor location (Figures 3.0 and 4.0) is primarily intended to house a thermocouple. Two short lengths of dissimilar metals are twisted together at one end to form the thermocouple contact. This twisted end sits inside the long slot making up the thermocouple channel with the loose wire ends attached to the thermocouple connection points with conductive epoxy. Using the same system employed for making electrical connections to the detectors, signal wires are connected to the substrates and thus to the thermocouple.

Cost Reduction

Beyond the use of inexpensive construction materials, the substrate design was also developed for low cost. The detector and electrical connection layout is designed to utilize symmetry instead of using three different substrate designs. A single base substrate design along with a single mask for electrodes serves for both the anode and cathode sides of the device without any modifications.

Neutron Reactive Material Deposition

The substrate and electrode design had to accommodate a means to apply different neutron reactive coatings without causing cross contamination. The design solution accomplished this through the electrode design. Since two identical substrates are used for the cathode and anode, each substrate may be coated by only one neutron reactive material. This keeps a substrate coated with one material from needing to be inserted in the electroplating bath of the second material. Therefore, the differing fissionable materials never come in contact. The electrode design also placed one electrode further to one side of the substrate than all other electrodes, which is shown in Figure 3 with the upper electrode having the greatest separation of all other electrodes. Originally the feature was used during the electroplating of the neutron reactive materials by only dipping this electrode into the electrolytic solution bath. However, due to the surface tension of the solution, the entire device was enveloped by the solution instead of only the one electrode being immersed into the solution. Still, the electrolysis chemically binds the neutron reactive material to the energized electrode. The remaining material may then be washed off the rest of the substrate and off of the other non-energized electrodes.

DETECTOR CONSTRUCTION

As previously described, different features are built into the MPFD^3-T in order to satisfy the design constraints for use as in-core detectors. Prototype construction allowed for processes and equipment to be developed for the final assembly of the MPFD^3-T. Described in the

following chapter are those construction steps, from substrate preparation to loading the detectors into their aluminum housings, for in-core deployment.

Electrical Contact Evaporation

Once the substrates had been cleaned using trichloroethylene (TCE), acetone, isopropyl alcohol, and deionized (DI) water process, the electrodes could be evaporated onto the substrates. In order to define the electrode patterns a shadow mask (Figure 1c) was developed. The shadow mask was mounted to a substrate holder (Figure 1d) in which the combination allowed for the evaporation of eight substrates each. Since the existing electron beam (e-beam) evaporator (Figure 1b) mount could hold two of these masks, a total of four holders and masks were constructed. This allowed one set to be cleaned and loaded with substrates while the other set was in the evaporator. The electrodes were suppose to all be built using a 100 Å layer of titanium followed by a 10000 Å layer of platinum. The thin layer of titanium was used in order to enhance adhesion between the alumina and the platinum.

Minor problems were encountered during this process. The first problem was due to the difficulty in aligning the masks to the substrate holders. Addition of alignment holes would have greatly eased this problem. An additional problem is that we suspect the masks were expanding due to being heated during evaporation. This caused the mask

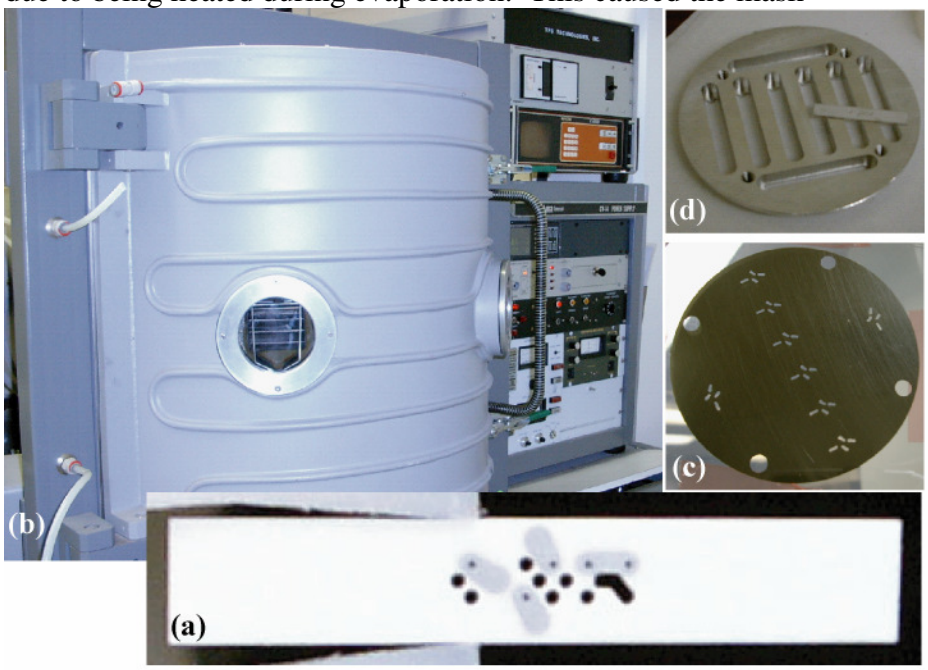

Figure 1: (a) Electrodes were deposited on the substrates using the (b) S.M.A.R.T. Lab's electron beam evaporator. The pattern was defined by a (c) shadow mask which was attached to the bottom of a (d) substrate holder.

to separate from the holder and thus the substrates would slip between the mask and the holders. The result was several "smeared" contacts due to the moving substrates. Applying a small amount of epoxy between the mask and holder helped remedy this problem. However, the addition of other mounting screws or incorporation of the mask into the holder would have been a preferred solution.

Annealing the Electrical Contacts

After evaporation, the platinum contacts have a much higher resistivity than that of bulk platinum due to a large number of structural defects. Most of the defects are due to the amorphous deposition with numerous voids in the bulk structure. Through the use of heat treatment, these defects can be annealed out and the overall resistivity lowered. Figure 2 shows the results of a study by Lourenco, et al, where the resistivity of two different coating thicknesses were measured after increasing heat treatment temperatures [40]. For this analysis, the heat treatment was performed at 100°C increments for 1 hour each. After each increment, the sample was allowed to cool to room temperature and the resistivity was tested. Analysis shows that the resistivity was lowered by heat treatments up to 900°C. The resistivity was found to be stable after this treatment and was within 4% of the bulk value of 1.042×10^{-7} Ω m at 22°C. Further evidence of the reduction of defects is shown by a decrease in thickness as the voids are removed [40].

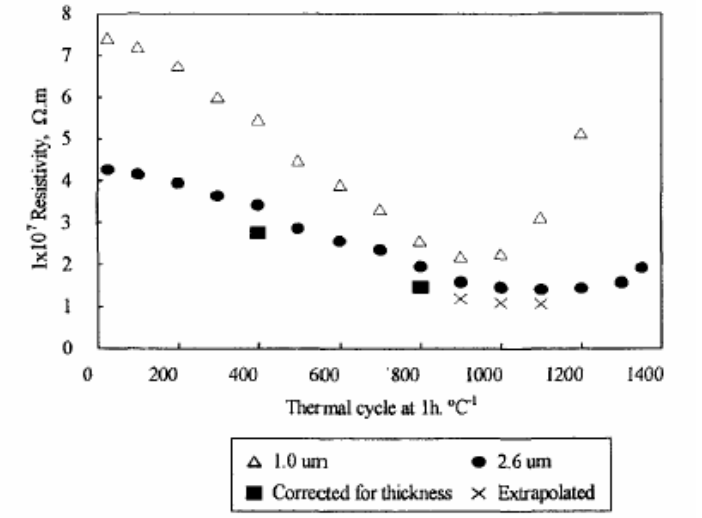

Figure 2: Resistivity variation of two evaporated platinum strips after heat treatments. Extrapolated and corrected for thickness data takes into account the decrease in thickness after heat treatments [40].

Figure 3: Nytech oven with old malfunctioning controller system. Internal area with new shelving shown.

Figure 4: Nytech oven with new controller and inert gas injection line.

The initial platinum contacts were deposited at only 1000 Å instead of the desired 10000 Å. The resistance of these coatings started at 20 Ω and after the heat treatment the resistance rose to 300 Ω. This rise in resistance is due to the platinum settling into the rough surface of the alumina substrate. The platinum was thin enough to cause separations between sections of the coating. In order to correct this problem, the coatings were evaporated again with 100 Å of titanium and 12000 Å of platinum, which was the maximum that could be deposited at one time due to measurement limitations. The new coatings initially had an average resistance of 2.13 Ω and after the heat treatment the resistance was lowered to an average of 0.855 Ω.

Figure 5: Mr. Cylinder system for automatically switching between argon gas bottles for the annealing oven.

In order to complete the 900°C heat treatment, a small oven was modified to handle all of the operations needed throughout the detector construction process. The modifications included the replacement of the old controller system with an Omega CN9600 controller and solid state relay. The oven had a slow thermal sensor response time due to a large insulated thermocouple, which caused the controller to oscillate. This problem was solved by replacing the sensor with a smaller and faster responding thermocouple located closer to the wall of the oven. The controller was also manually tuned to provide a smoother temperature profile. Another modification was the addition of a stainless steel shelving system to accommodate numerous samples.

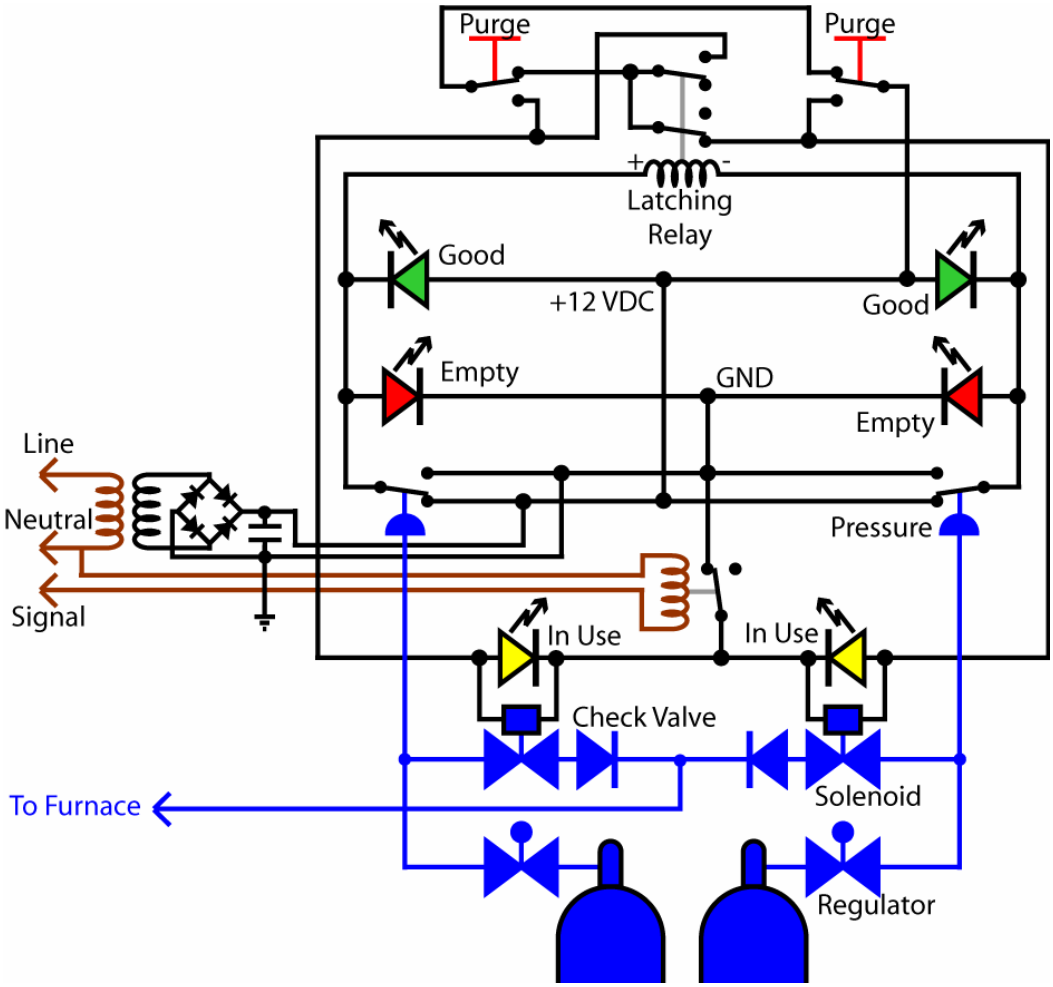

Figure 6: Flow schematic and circuitry diagram for Mr. Cylinder.

In order to keep from oxidizing the contacts and the neutron reactive materials, the atmosphere within the oven must be purged by an inert gas, such as argon. A gas control system, dubbed "Mr. Cylinder," (Figure 5) was constructed to operate with the Nytec annealing oven controller by activating an argon gas flow when the oven temperature exceeds 35°C. The primary purpose of Mr. Cylinder is to maintain an argon atmosphere throughout an entire thermal process. Since some of the processes take nearly a day to run, a partially used gas cylinder would be drained before completion of the process. Mr. Cylinder allows two cylinders to be connected for gas flow but allows only one cylinder to be drained at a time. Upon depletion a cylinder, Mr. Cylinder switches gas flow to the other cylinder and sets an "empty" indicator light for the previous cylinder. The empty cylinder may then be switched out for a new cylinder. The control circuitry ensures that a cylinder is drained before switching to the new cylinder, thus ensuring the longest possible run time for the oven. The Mr. Cylinder front panel also has indicator lights showing when each cylinder still has useful ("good") pressure, or is full, and when it is "in use". A "purge" switch allows the user to manually drain a cylinder line prior to removing the regulator from the cylinder for cylinder replacement. The automatic selection circuitry is based on two diaphragm pressure switches and a double pole, double throw (DPDT) latching relay. The relay's state controls the gas flow through the electrically actuated solenoids.

The circuitry diagram and flow schematic of Mr. Cylinder and its connection to the Nytec annealing oven are shown in Figure 6.

Electroplating of Neutron Reactive Materials

Once the electrodes are annealed, the neutron reactive material may be applied to them. The calibration of the MPFDs is dependent on the amount of material deposited and the uniformity of its thickness. In order to accomplish this with consistent results for all 150 coatings, the Automated System for the Consistent Electroplating of Fissionable Isotopes (ASCEFI) was designed and built. ASCEFI is made from six primary components which are designed to minimize fluctuations in the variables that affect electroplating results. These components are the substrate cart, the plating bath, the plating chamber, the hot water bath and electrolyte storage, the electrolyte flow subsystem, and the system controller.

Figure 7: The Automated System for the Consistent Electroplating of Fissionable Isotopes.

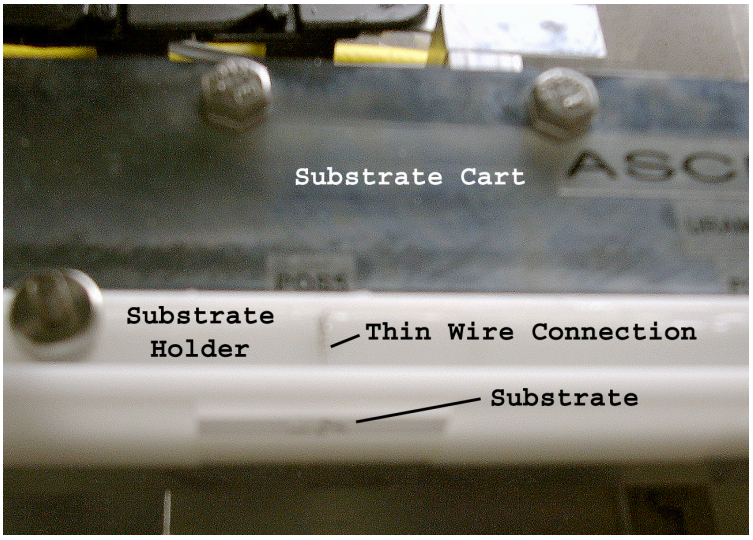

Figure 8: Substrate cart of ASCEFI with the attached substrate holder loaded with a substrate. The substrate is held in place and is connected to the electroplating circuit through a thin wire that goes through the base of the holder.

The first part of the system is the substrate cart. It is designed to move ten substrates, five for uranium and five for thorium plating, into the plating chamber, and then aligns the proper substrate with the plating bath for coating application. The plating chamber is a dual purpose structure built from Plexiglas. The primary purpose is to restrict airflow and thermal losses around the plating bath while keeping dust and foreign objects out of the solution. The secondary purpose is to limit radioactive contamination of persons working on the system and to also limit any spread of contamination outside of the plating chamber. The entire system, except for the controller, is also constructed inside a fume hood for added protection. All fume hood exhaust is run through a HEPA filter to scrub out any airborne particulates.

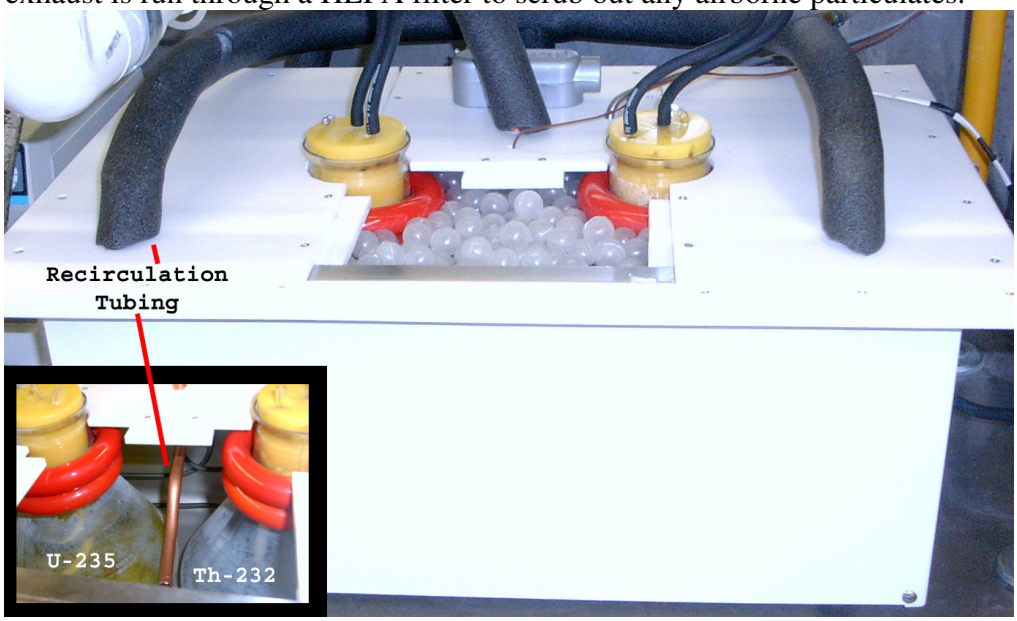

Figure 9: Hot water bath with uranium and thorium electrolytic solutions loaded.

Control over the electrolytic solution is primarily provided by the flow system and the hot water bath. The hot water bath is an insulated stainless steel tub which houses two 2.8 L Nalgene Erlenmeyer flasks, one with uranium solution and the other with thorium solution. The tub also houses a submerged inconnel resistive heating element, a thermocouple, a water level float sensor, and a water replacement tube. The heater and thermocouple are controlled and monitored through an Omega CN9600 controller which is integrated into the system controller. For added safety, the temperature may only be adjusted through the system controller by a logged in user and not through the CN9600 buttons. In order to ensure an even temperature, the water inside of the tub is circulated by an external high temperature pump. Two layers of hollow plastic balls cover the water surface to help minimize heat loss. A polypropylene cover is also used to seal the tub and provide support for the different components. Even with these heat loss reducers in place, some of the water will evaporate. To avoid running the system dry a water level float sensor has been installed. When the water level starts to become low the sensor energizes a solenoid connected to a point-of-use hot water heater. Two lines are connected to this solenoid. One goes to the water box for refilling while the second is connected to the drain. Once the solenoid closes (de-energized) the refill line is drained by gravity through the drain line. This ensures that room temperature water trapped in the line does not enter the water box and thus lowers the water box temperature. Instead, only water that is close to the water box temperature is added.

Figure 10: Peristaltic pump for controlling electrolytic solution flow.

Figure 11: Sensor port for loading a pH and temperature sensor in the electrolytic flow path or for adding chemicals to the solution.

Three Pyrex tubes pierce the rubber stopper of the Erlenmeyer flasks. One tube acts as a vent to ensure pressure equalization and has a curved tip to minimize debris entering the solution. Another tube continues to the bottom of the flask and is used for sucking the solution from the flask. The last tube stops just after the stopper (like the vent tube) and is used to drain the solution back into the flask. A single peristaltic pump is connected to both sets of suction tubes. From here the tubes connect to a solenoid pinch valve which directs the flow to either the plating bath or back to the drain. Solution flowed into the plating bath spills over and flows back

into the same drain line and then back to the holding flask. Allowing the solution to only flow to the drain, and not to the plating bath, causes the solution to be mixed. The suction path also has a sensor port which allows a pH meter and thermocouple to be placed into the solution flow. This port also allows the addition of pH buffers to the solution in order to ensure proper pH.

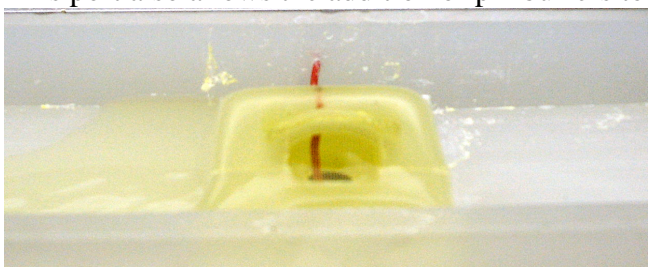

Figure 12: Uranium plating bath with flowing solution. The red wire connects to the platinum mesh through which the electrolytic solution flows.

Figure 13: ASCEFI controller which monitors and controls all system components.

The brainpower behind ASCEFI is its controller. A Micro-Bit 3000 controller provides a user command entry and visual output interface. Its custom programmed microcontroller then interfaces with the CN9600 and custom designed circuitry to coordinate and monitor full system operations. Through this controller, the user specifies the plating temperature, the solution mixing time, the plating bath temperature equalizing time, the surface area to be plated onto, the current density rate to be achieved, the locations to be plated, and the total current density to be plated at each location. The controller begins the plating operation by setting the water bath temperature via an RS232 connection to the CN9600. The substrate cart is then raised and moved to the hold position. The controller and CN9600 continue communications to monitor the water bath temperature. Once the desired temperature has been reached the peristaltic pump is started to mix the solutions. After the mix time has expired, the solution to be plated flows through its plating bath. This continues for the preset time and will wait, if necessary, until the

water bath is at its preset temperature. The plating bath is then drained (prevents splashing later) and the substrate cart moves to locate the selected substrate directly above the plating bath. The cart is then lowered, the bath is refilled, and the electroplating begins.

The controller manages the electroplating process by setting a voltage which is proportional to the current density desired. An operational amplifier compares this voltage to a voltage produced across a known series resistance in electroplating circuit. The operational amplifier controls the current by varying the voltage difference between the electrode on the substrate and a platinum mesh located in the solution flow path inside the plating bath. The total current density is monitored on the custom circuit board through a voltage-to-frequency converter (VFC) and a series of counters and registers. The registers are loaded with a 24-bit number representing the total current to be applied prior to starting the electroplating process. During the electroplating process, the VFC generates a clock signal for the counters which is proportional to the current density. A relay is immediately switched once the counters are equivalent to the registers, which disconnects from the DAC and sets the plating voltage to zero by shorting to the substrate electrode voltage. The plating bath is then drained and the substrate cart is raised. Once the drying time has expired the cart is moved to the next location selected for electroplating.

While the thickness calculations were presented in 0, details of the chemistry, voltages, and current densities are held under a non-disclosure agreement with Reuter-Stokes. It was through this agreement and with the help of their radiological chemist, Kimberly Hoffert, that we were able to do our own fissionable material electroplating. However, the nondisclosure agreement does not allow for additional information regarding the electroplating process to be included.

Substrate Assembly

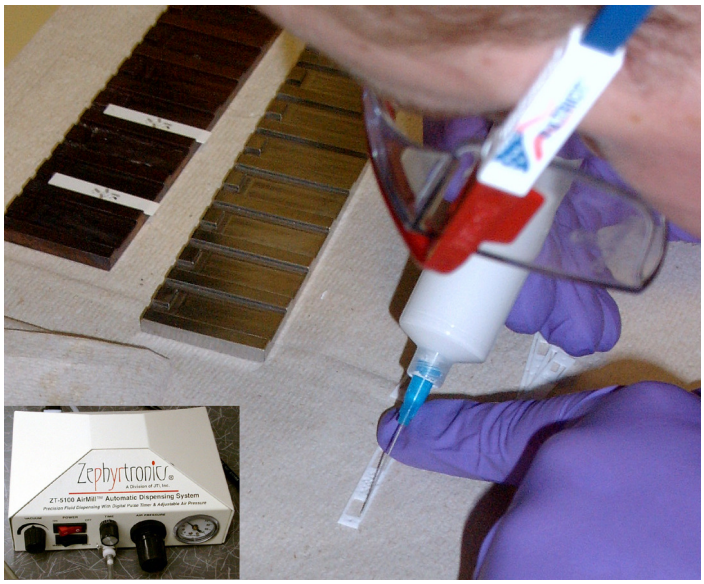

Figure 14: Application of the alumina epoxy using the Zephyrtronics Air Mill dispensing system.

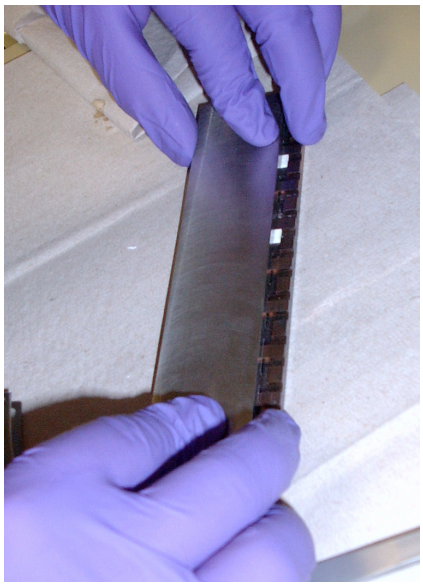

Figure 15: Interdigitated plates for aligning the substrate pieces and pressing them together.

The three substrate pieces are assembled together using an alumina-based epoxy. The Aremco 503-VFG-C epoxy is applied to the cavity substrate using a Zephyrtronics Air Mill

automated dispensing system. The system allows very minute amounts of epoxy to be applied in a precisely controlled manner. Once the entire face is covered it is attached to one of the base substrates and aligned using an interdigitated set of alignment plates. This process of applying the epoxy and aligning the substrates is repeated for the other base substrate. The assembled detectors and alignment plates go through the Aremco suggested heat treatment cycle for 2 hour increments at 93.3°C (200°F), 260°C (500°F), and 371.1°C (700°F) in the annealing oven [41]. During this process the binders in the epoxy are burned out and a nearly pure alumina adhesive remains.

Adding Fill Gas and Hermetically Sealing the MPFDs

Figure 16: Custom built glove box and vacuum system for the back filling of the detectors with pure argon.

Figure 17: Direct drive rotary vane vacuum pump used in the backfilling system.

A specialized glove box and vacuum system is used to fill the detector chambers with pure argon and to trap it inside the detectors. This is done by taking the assembled substrates and loading them inside the vacuum chamber located at the back of the glove box. With the glove box fill valve closed and the argon backfilling valve closed, the chamber can be evacuated using a direct drive rotary vane vacuum pump by opening the vacuum valve. A thermocouple vacuum gauge is used to monitor the vacuum level in the chamber. Once the chamber has been held at a vacuum level of 300 mTorr or less for at least 30 minutes, the vacuum valve is closed. The chamber is then slowly flooded by ultra high purity (UHP) argon up to a pressure just slightly above atmospheric pressure. The cycle of applying the vacuum and backfilling with argon is repeated at least four more times to ensure as high a purity of fill gas as possible. With the argon backfilling valve open, the glove box is flooded with argon by opening the glove box fill valve. After allowing the argon to flow for at least one hour, the end cap of the vacuum chamber containing the glove box fill valve is removed and the detectors are removed from the vacuum chamber. The Zephyrtronics Air Mill used to assemble the substrates is used with an Aremco 813A alumina based epoxy to seal the gas fill channels. This epoxy is used due to its ability to cure at room temperature for 24 hours. In order to ensure total curing of the epoxy

plugs the substrates undergo a follow up heat treatment of 93.3°C (200°F) for 3 hours under the argon atmosphere of the annealing oven [41].

Connecting Wires

A specialized tool was built to connect the wires to the detectors. This wire winding system (Figure 19) is designed to load a specialized spool with 6 feet of wire. The length of wire is controlled by using a 75 rpm motor and a timer relay. A slot located in the top center of the spool allows an assembled MPFD to be erected vertically in the slot. Each wire is then disconnected from its source spool and is fed through the wire connection pocket. The Zephyrtronics Air Mill is used to apply an Aremco 597A silver-based epoxy or an Aremco 598A nickel-based epoxy inside the pocket to provide an electrical connection between the wire and the electrode along with providing mechanical adhesive bond between them. The wire wound spool and the detector are baked out in the annealing oven for 2 hours at room temperature followed by a 2 hour heat treatment at 93.3°C (200°F) [42]. A flat surface located opposite the slot in the spool allows the spool and detector to be loaded into the oven without rolling around. Once complete, the wires are unwound from the spool for insertion into the alumina insulation tubes and then into the in-core housing.

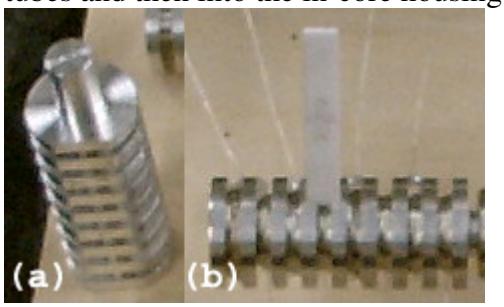

Figure 18: The wire winding spool contains cylindrical slots for each wire, (b) a slot for hold an assembled MPFD vertical, and (a) a bottom flat to keep the spool from rolling inside the annealing oven.

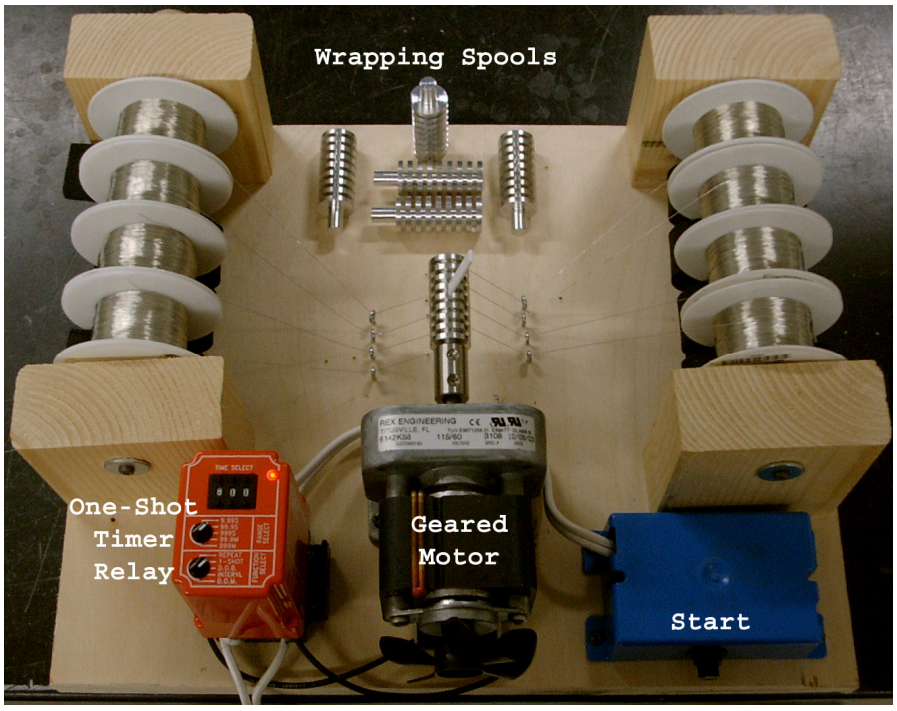

Figure 19: Custom built wire winding system with an MPFD loaded in the wrapping spool slot.

In-Core Housing

Figure 20: Long water tank used for leak checking each flux probe tube.

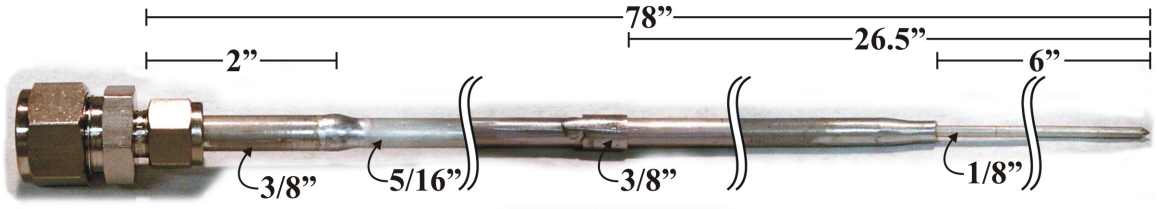

Figure 21: Flux probe design showing (from right to left) the 1/8” lower grid plate pin which is welded inside a 5/16” (0.030” wall) aluminum tube. A 3/8” collar is welded 26.5” from the bottom to provide an indexing guide to the top grid plate. Another 3/8” collar is added to the end of the tube to support a 3/8” to 5/8” Swagelok coupler for connection to a stainless steel tube.

The single greatest difficulty in getting data from prototype detectors was due to the in-core housings. Several different tubes were constructed with nearly all of them becoming flooded with water due to small, often pinhole, leaks. Aluminum was used due to its low activation cross section and its short decay half-life, thus allowing assemblies to be removed for inspection after being irradiated. Different designs included an underwater preamplifier box, a single bent tube with a screw-in bottom cap, and finally an assembly of pipe and pipe fittings.

The final design was simply 3/4 inch aluminum pipe ordered through McMaster-Carr, and it did not leak. Unfortunately, the 8 mm diameter specialized tubes needed for in-core flux probe deployment require custom manufacturing. Initially, leaks also plagued these tubes and it was finally determined that the problems were due to the method used to weld the tube parts together. The DC type welder would get impurities trapped in the weld. As the weld would cool the impurities would move to the surface and leave behind pinhole trails. To solve this, a push-pull, or square wave, welder was found which would pull the impurities out of the weld as the weld was being made. To ensure that the tubes would not leak, each one was pressurized with argon at 40 psi, over four times that seen in the reactor core, and submersed in a long water tank. The tubes were thoroughly inspected for bubbles before being accepted for use as in-core flux probes.

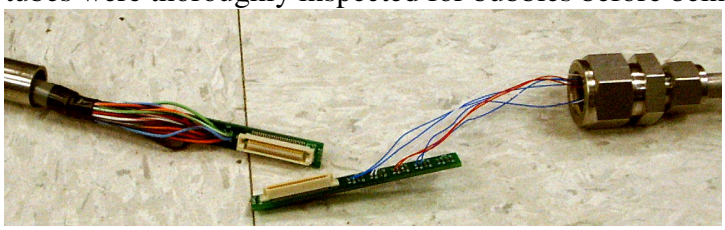

Figure 22: Connector circuit boards for switching wiring from the bare 30 AWG wiring (prototype insulated wiring shown) in the flux probe tube to the shielded 24 AWG wiring in the 5/8" stainless steel tubing.

The flux probe tubes are designed to hold the tube vertical in the core by using both the upper grid plate 8 mm (5/16") diameter holes and the lower grid plate 4 mm (5/32") diameter holes. The tube also has a stop which rests on the upper grid plate and aligns the detectors vertically with the core. This stop is provided by a short 3/8" collar tack welded to the 5/16" tubing. The overall chamber length is six feet in order to significantly reduce the gamma and neutron field from the reactor while not being too long to increase costs due to the alumina insulation. A 3/8" sleeve is welded to the top of the tube so a Swagelok 3/8" to 5/8" connector can be attached. At this point the tube is connected to a 5/8" stainless steel tube which incorporates a set of bends to prevent radiation streaming. The wiring is also changed from bare 30 AWG wire to a shielded 30 conductor 24 (7/30) AWG cable via a specially designed connector and circuit board. The circuit board connector system fits inside the 5/8" tubing and allows probes to be tested and switched out without desoldering or cutting wires. The shielding around the cable acts as a double electrical shield with the tubing while remaining isolated from the tubing to break any ground loops between the electronics and the reactor core and tank.

NEAR-CORE AND IN-CORE TESTING

Several prototype MPFDs have been constructed and tested at the Kansas State University TRIGA Reactor, both near-core and in-core. The experimental results shown in this chapter not only proves that the MPFD concept is feasible but also demonstrates the future potential of the technology.

Beamport Testing

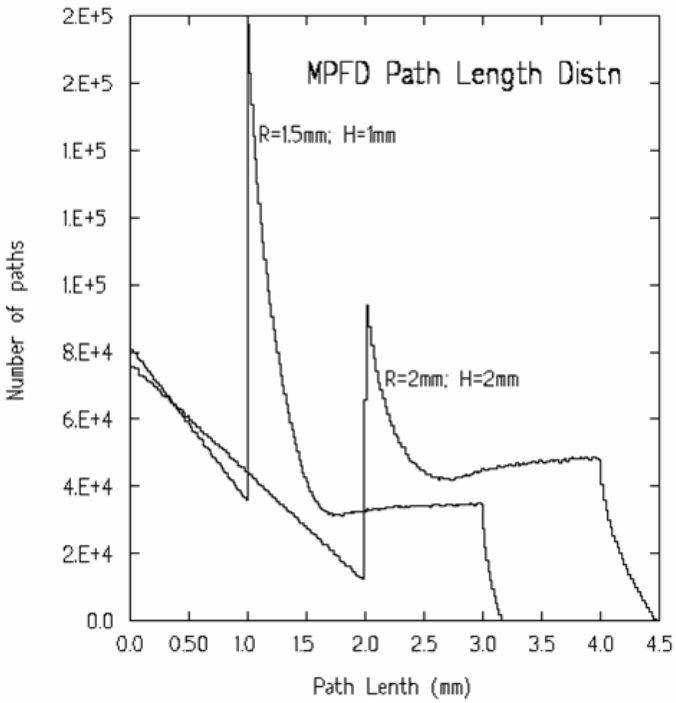

Figure 1: Theoretical pulse height spectrum based on fission product path length through two different detector sizes [1].

The theoretical pulse height spectrum can be simulated by finding the fission product path length distribution inside the detector chamber. As shown in Figure 2, the energy deposition per unit path length is nearly linear for small chamber widths and thus the simulation is a valid theoretical approximation to the pulse height spectrum. Figure 1 shows the simulation results for a 3 mm diameter by 1 mm thick detector chamber [1]. Beamport tests of a prototype detector similar to that of Figure 3 yielded the spectrum shown in Figure 2. The neutron field at the detector was approximately 1.6×10^{6} n cm^{-2} s^{-1} and had a gamma ray dose rate of 10 R h^{-1}. It should be noted how similar the experimental data and the simulation are to each other in which a peak is created along with a tail that continues to the right of the peak.

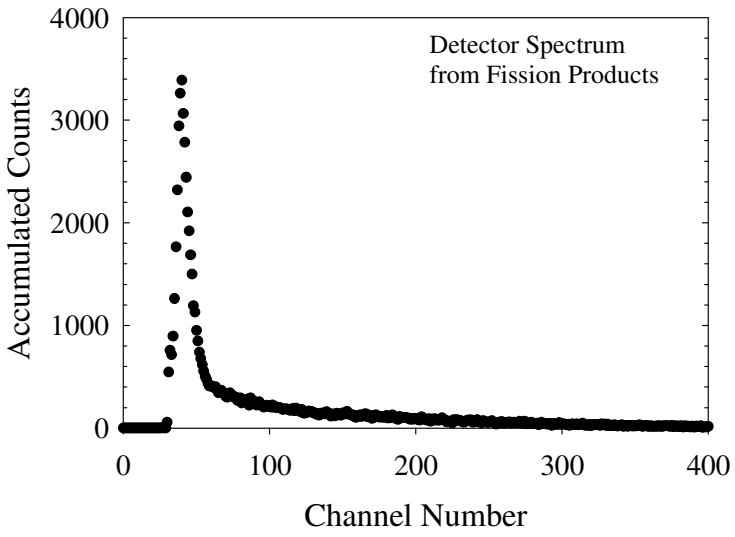

Figure 2: Beamport differential pulse height spectrum for a natural uranium coated MPFD with 3 mm diameter by 1 mm wide chamber [1,14].

Central Thimble Testing

A prototype MPFD, similar in design to the detector shown in Figure 5, was tested in the center of the central thimble of the nuclear reactor core. In the central thimble, the full power (250 kW) slow neutron flux is 1.0×10^{13} n cm^{-2} s^{-1} and fast neutron flux is 1.2×10^{13} fast n cm^{-2} s^{-1} with a gamma dose rate 2.5×10^{4} rad s^{-1} [29]. The MPFD was tested through power levels from 10 mW up to 200 kW with the detector being operated in pulse-mode through this entire power range. The log-log plot shown in Figure 3 demonstrates the linearity of the detectors over slow neutron fluxes from 4×10^{5} n cm^{-2} s^{-1} to 8×10^{12} n cm^{-2} s^{-1}, over 7 orders of magnitude. Apparent nonlinearities at low power levels can be explained by the combination of source neutrons and limitations of reactor instrumentation and controllability at low power. Figure 4 shows that at high power levels the deadtime effects remain acceptable with only 24% deadtime at 200 kW [15]. In addition to the excellent pulse-mode linearity of this detector, it was operated with twenty feet of wire between the MPFD and an Ortec 142B preamplifier. Even with cabling of this length, the difference between the background noise and the neutron induced signals allows for simple discrimination.

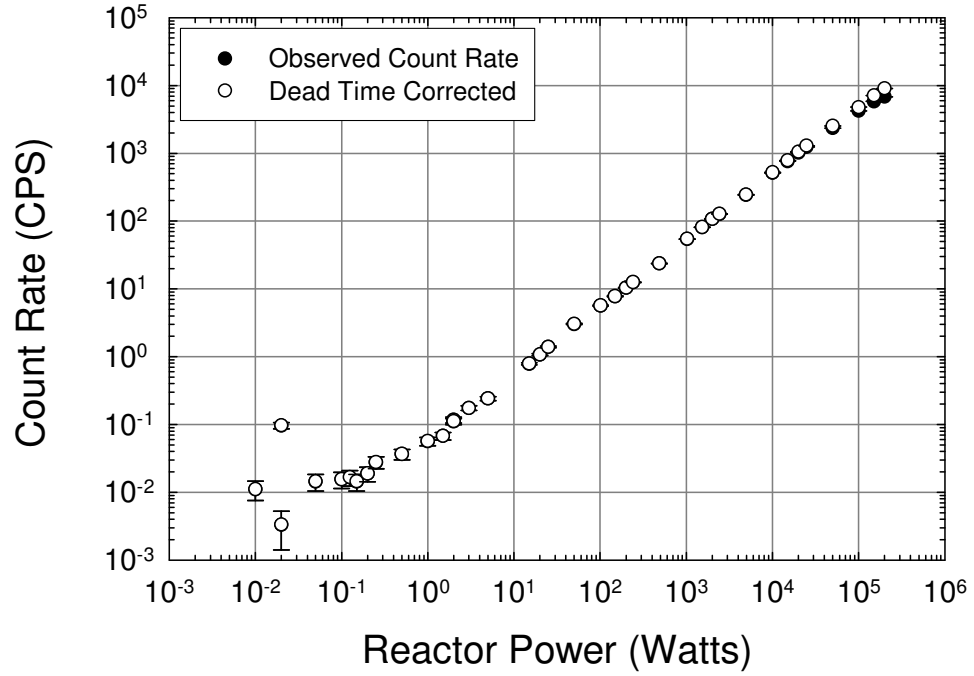

Figure 3: In-core central thimble test results from 10 mW to 200 kW with detector operated in pulse-mode [15].

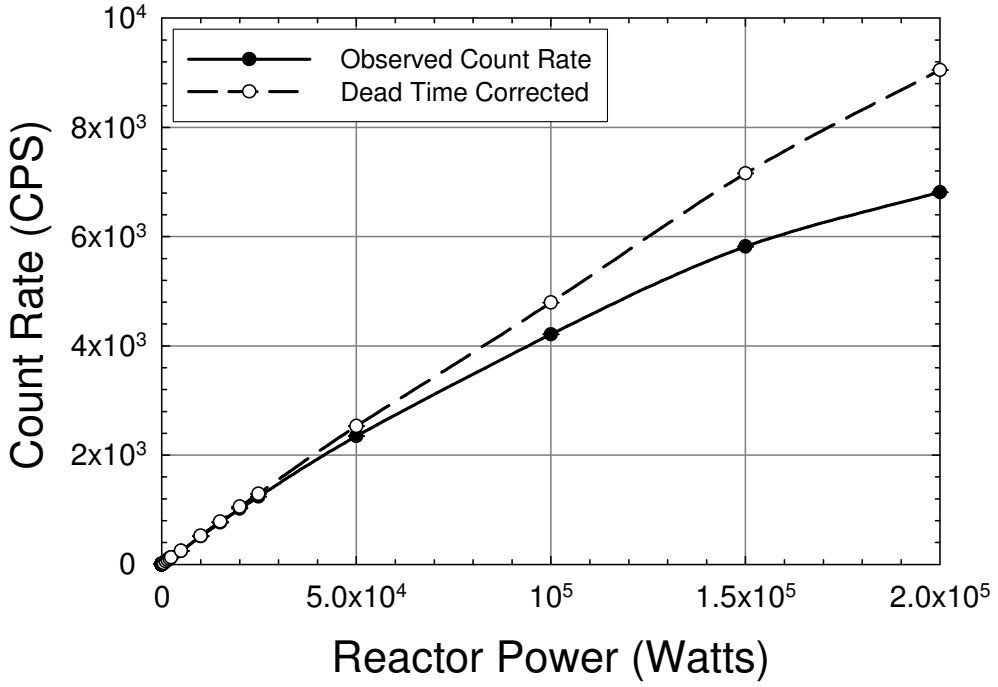

Figure 4: Linear plot of Figure 3 showing a deadtime of only 24% at 200 kW or 9.6×10^{12} slow n cm^{-2} s^{-1} flux [15].

Duration Testing

An initial test to show the radiation hardness of the MPFDs was conducted using a prototype detector first tested in the southeast beamport, then tested in the central thimble of the reactor core, followed by another test in the southeast beamport. The first beamport test showed that the detector was producing pulses as expected. Once these tests were completed, the detector was loaded into the central thimble via a specially designed aluminum tube. Tests found that the tube had quickly flooded and thus rendered the detector unusable. The prototype MPFD was left in the core for several months and while the reactor did not perform a lot of operations during that time, the detector did receive a total neutron fluence greater than 6×10^{16} n cm^{-2} while also being immersed in water. The prototype MPFD was removed from the core, dried out, and tested again in the southeast beamport. In these tests the detector responded to the beamport neutrons the same as it had in the prior beamport tests.

MPFD^3-T Prototype Testing

In order to prove the workability of the MPFD^3-T design and to verify that ASCEFI was in fact depositing neutron reactive material, a natural uranium coated MPFD^3-T set of substrates was assembled and tested in the reactor core. Four different coating thicknesses were applied to form two sets of MPFD^3-T which were constructed using most of the methods described in 0. Exceptions to these methods were the process of adding fill gas and the epoxies used to seal the substrates and connect the wires. A 2-ton epoxy from a local hardware store was utilized to seal the substrates together. Instead of using epoxy plugs to seal in the fill gas, the gas was trapped inside when the substrates were sealed together inside of an argon filled glove box. The wires were connected to the substrate contacts using solder paste. These processing exceptions allowed the detectors to be constructed in a significantly shorter amount of time and they have been experimentally proven to work in previous prototype tests. Using the cabling setup described in sections 0 and 0, the detectors were wired to an Ortec 142IH preamplifier via 40 feet of cable. Through this setup the preamplifier sees a detector capacitance of approximately 900 pF. Figure 5 is an oscilloscope screen capture showing a neutron induced pulse output of the preamplifier and the shaped output pulse from the Canberra 2022 amplifier. It should be noted from this screen capture that the preamplifier output pulse has a peak to peak voltage of 791 mV and with a shaping time of 8 μs and a gain of 3 yields the amplified pulse of 5.87 V. In comparison, Figure 6

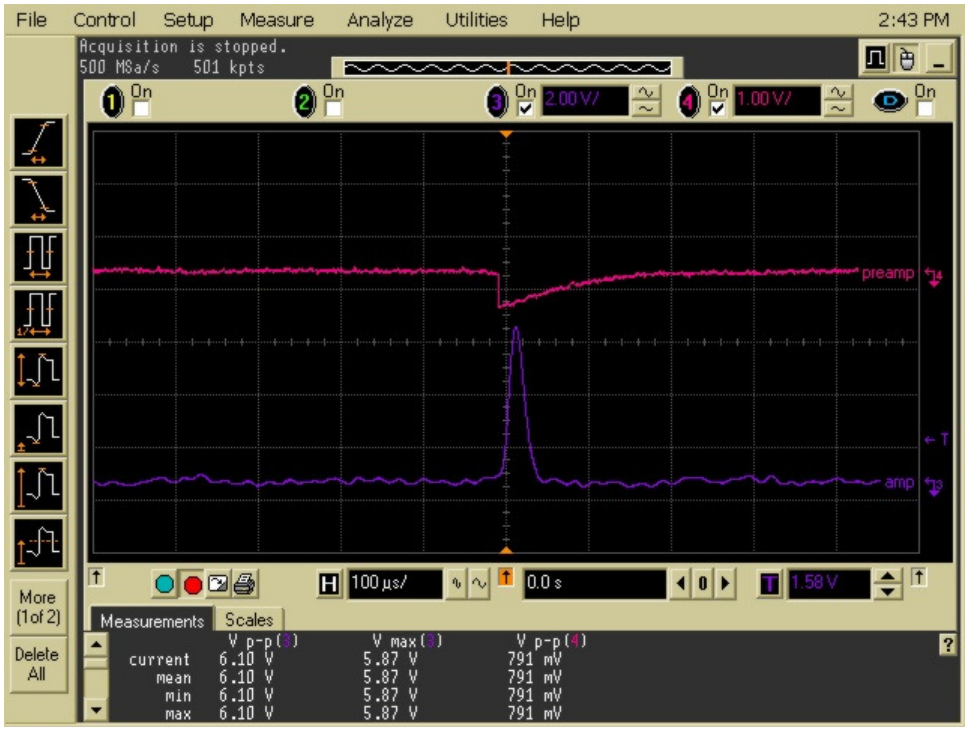

Figure 5: Oscilloscope screen capture showing preamplifier (top) and amplifier (bottom) outputs during in-core tests.

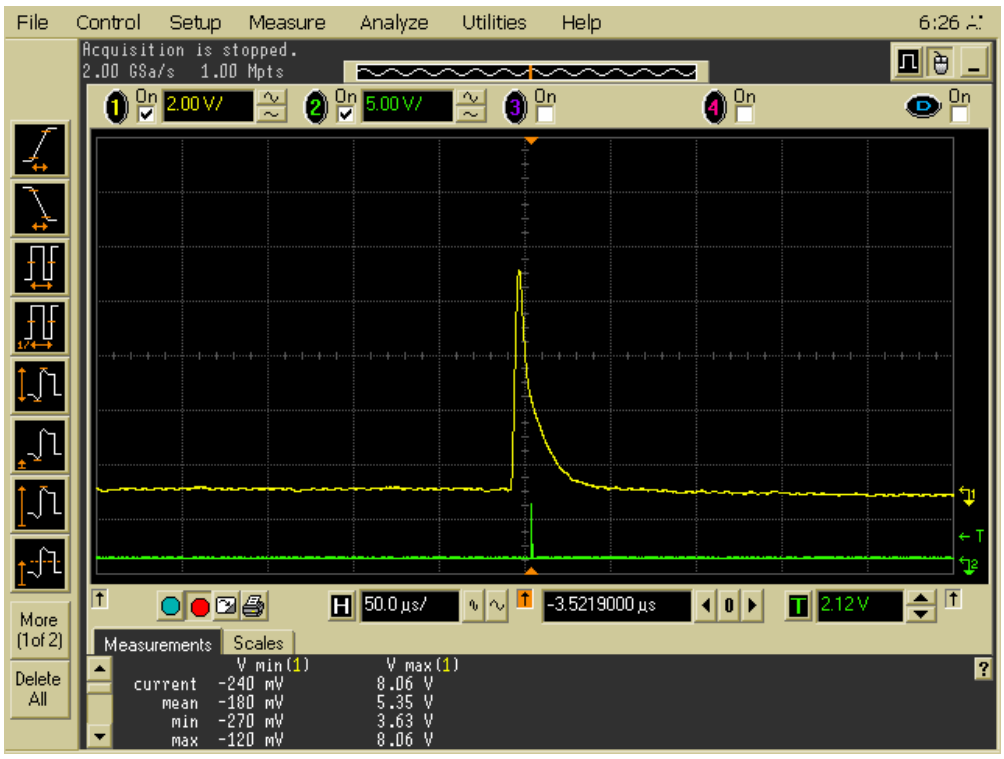

Figure 6: Oscilloscope screen capture showing preamplifier (top) and discriminator (bottom) outputs using an Amptek A250 preamplifier closely coupled to an MPFD tested at the southeast beamport.

shows a neutron induced pulse output from an Amptek A250 preamplifier and a digital pulse from a discriminator. The characteristic tail-pulse shaped signal is produced by both preamplifiers with the differences between them being due to differing RC time constants, with the largest contributor being the detector capacitance. Being that the Amptek preamplifier was closely coupled to the detector the large line capacitance found in the in-core test is not present and thus the overall capacitance was approximately 100 times smaller.

Figure 7 shows the collected differential pulse height spectrum of an in-core MPFD^3-T prototype coated with natural uranium through 10 coulombs of charge transfer. The bias supply for this device was set at 1000 VDC but the actual voltage on the detector was far less. This drop in voltage is due to a significantly large noise current which induces voltage losses in resistors present in both the bias supply and the preamplifier. The noise generated sine shaped, not tail-pulse shaped, pulses which generated amplified Gaussian pulses in comparable voltage heights up to those in the peak region shown in Figure 1. Due to this noise, the lower level discriminator (LLD) had to be set rather high and thus the differential pulse shape information below channel 793 is not available. However, the expected plateau to the right of the peak is visible.

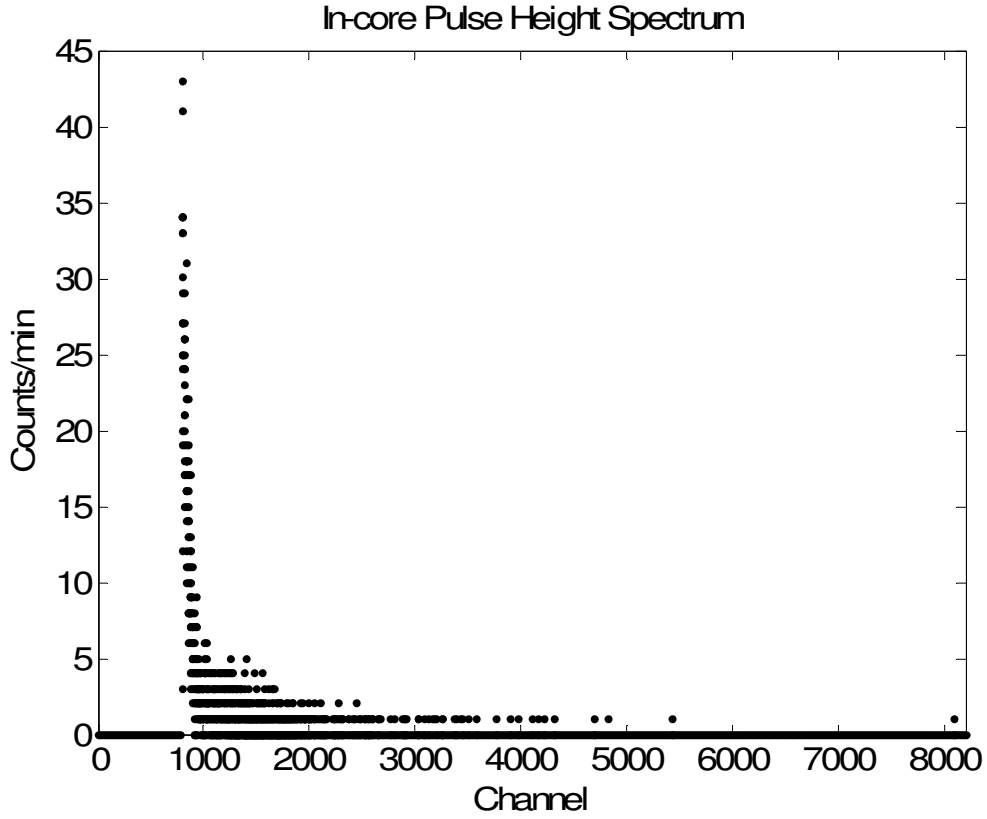

Figure 7: Differential pulse height spectrum of the MPFD with a bias of 1000 V.

FUTURE WORK

Micro-Pocket Fission Detectors have been successfully demonstrated as near-core and in-core neutron detectors. The equipment necessary to produce the MPFD^3-T is also developed.

While the prototypes have been shown to work there is still much to be done in order to complete the project goals and to fully characterize the performance abilities of the MPFD.

Full In-Core Array Deployment

The eventual project goal for the MPFD research is to develop and deploy an in-core array of real-time neutron flux monitors. Throughout the present work, the in-core array design constraints and design solutions of the MPFD^3-T and its method of deployment have been described. The planned MPFD array will consist of fifteen detector strings, one string per insertion tube, with five MPFD^3-Ts per string, or a total of 225 detectors, along with 75 thermocouples. From the array, 75 detectors will primarily provide slow neutron flux data while 75 other detectors will initially provide fast neutron flux data, and an additional 75 detectors will record the average gamma ray background contribution of the prior signals. Specialized electronics must be designed and built in order to collect real time data from all of these detectors simultaneously in pulse, current, and mean-squared voltage (MSV) modes of operation. Software must also be created to record and process the data collected by the electronics. This data will be used to perform back-calculations to generate a 3-dimensional power map of the core. The overall goal of this entire project is the development of detectors and numerical methods to observe the real-time shift in neutron flux and power generation of the reactor through operational transients, including the fast power transient of a reactor pulse.

High Temperature Testing

The Kansas State University TRIGA Reactor is limited to operating pool temperatures less than 48.9°C (120°F) which is far below the operational temperatures of BWR, PWR, and especially the Gen IV reactors which may reach 1000°C. However, it is believed that MPFD technology will greatly enhance the operation efficiency, control, and safety of power reactors and therefore the detectors must be tested at high operating temperatures. While efforts have been made to select the MPFD^3-T construction materials to withstand temperatures greater than 1000°C, as well as have similar thermal expansion coefficients, the electrical connection and wiring materials are thus far the expected thermal limiting conditions. The Aremco 597A silver based epoxy and 598A nickel based epoxy have 649°C (1200°F) and 538°C (1000°F) temperature resistances, respectively [42]. Even though these temperatures fall below the 1000°C threshold, the binder system utilized in these epoxies should remain stable over 1000°C, however, Aremco will not certify the epoxies at this temperature due to the potential of oxidation [43]. A platinum ink (5542) from Electro Science has been located which will withstand temperatures in excess of 1000°C, but its mechanical properties have not been tested. Other possible solutions include wire bonding or welding, but these would both require modifications to the substrate designs.

The thermal testing of these detectors will determine whether the MPFD^3-T can be operated at and survive high temperatures. Extending this testing to use an oven in line with a beamport will also provide valuable information as to the temperature affects on the detector response.

Testing at Other Facilities

The long-term goal of using MPFDs in power reactors necessitates that tests be conducted in reactor facilities in addition to the Kansas State University TRIGA Reactor. Selection of these reactors can be done in order to test the limits of MPFD designs. Reactors

such as the Advanced Test Reactor (ATR) and the High Flux Isotope Reactor (HFIR) are two possible research reactors which could be utilized to perform extreme in-core testing.

Expanded Modeling

The detector lifetime analysis and optimization methods described in Sections 0 and 0 have limitations and are only developed as a nearly ideal study. In reality, reactors do not operate at full power continuously for their entire life, which relaxes the first of many assumptions utilized in the optimization method. In order to verify the validity of this assumption, trials must be made with power fluctuations to determine the optimization band for a coating mixture. The optimization method of Section 0 also assumes that nuclides being generated from the fission products do not have an affect on detector performance. While the quantities of these nuclides should be negligible, it could be beneficial to verify that these quantities do remain negligible throughout the decades of detector operation. Evaluation of the fission product buildups will also help characterize the affects on the fill gas purity.

The reactor flux profile model was also developed through limiting approximations. While the general shape and integral flux correspond to experimental measurements as best as possible, a more rigorous analysis may yield improved results. The most significant improvements would include temperature effects, profile shifting over core lifetime, and whole core flux variations. The extreme temperatures utilized in power reactors will cause a shift in the reactor flux profile, but most importantly will cause Doppler broadening in the cross sections of the neutron reactive coatings. This effect causes the peaks in the cross sections to lower and become wider (area is conserved) which may change the detector's response. Since the modeling is carried out over numerous years, the effects of operation on the core should also be taken into account. As with the detector coating material, which is very similar or identical to the reactor fuel, the fuel will undergo transmutations, and thus the reactor response does change over its lifetime.

The current optimization method takes into account only the neutron flux at a particular point in the reactor, and indicates the best neutron reactive coating for use in that location. Using this method of optimization would then recommend that every detector be optimized for its specific location in the core. However, the long term goal is for these detectors to be mass produced for general use anywhere in a reactor. Therefore, improving the model to include optimization over a range of neutron flux profiles would be valuable.

CONCLUSION

Micro-Pocket Fission Detectors have shown both excellent theoretical capabilities and experimental performance as near-core and in-core real-time neutron radiation detectors. Their miniature size has proven to improve performance while also allowing for use of inexpensive materials and methods of construction. This miniature size also allows multiple detectors to be located between fuel elements which will be beneficial for future deployment of large three-dimensional detector arrays. Theoretical analysis has also shown that the detectors are capable of maintaining a flat response over the life of a core making them ideal for in-core use. Their design also allows for multiple types of neutron reactive coatings in order to unfold a rough neutron spectrum of the in-core neutron flux.

The development of the prototypes leading to and including the MPFD^3-T design has resulted in the construction of numerous tools to aid in the assembly of these neutron detectors. The most prominent of these tools is the Automated System for the Consistent Electroplating of

Fissionable Isotopes (ASCEFI). This system has demonstrated the ability to deposit uranium and thorium through both visual tests and in-core and near-core tests. Through additional tests it will be possible to determine the proper neutron reactive coating thickness for use in the Kansas State University TRIGA Reactor. Other tools include the shadow masks used for evaporation of the platinum contacts, the annealing oven and Mr. Cylinder which are utilized during many of the processing steps, and the glove box and vacuum system used to add fill gas to the detectors. Additional tools include the alignment plates for use while assembling the substrates, the wire wrapping tool, and the test chamber for checking the in-core housings for leaks. With all of these tools now in place, it will be possible to quickly and reliably produce the $MPFD^3$-T devices needed for the next phase of this research project.

This new evolutionary step in fission chamber design shows great potential as the next step towards the ideal in-core neutron detector. With these detectors now developed it will be possible to distribute a large array throughout the reactor core in order to produce the first three-dimensional array of detectors for real-time in-core neutron flux monitoring. However, work must still be done to design the electronics in order to couple with the detectors and to minimize noise inputs.

REFERENCES

[1] M.F. Ohmes, D.S. McGregor, J.K. Shultis, P.M. Whaley, A.S.M. Sabbir Ahmed, C.C. Bolinger, and T.C. Pinsent, "Development of Micro-Pocket Fission Detectors (MPFD) for near-core and in-core neutron flux monitoring," *Proceedings of the SPIE*, Vol. 5198, pp. 234-242, 2003.

[2] G.F. Knoll, *Radiation Detection and Measurement*, 3rd ed. New York: Wiley, 2000.

[3] "Fission chambers – general information," Centronic LTD, Radiation Detectors, Ref. 313/06, September 2002.

[4] J.K. Shultis and R.E. Faw, *Fundamentals of Nuclear Science and Engineering*, New York: Marcel Dekker, Inc., 2002.

[5] A. Rose, "Sputtered boron films on silicon surface barrier detectors," *Nuclear Instruments and Methods,* 52, pp. 166-170, 1967.

[6] A. Mireshghi, G. Cho, J.S. Drewery, W.S. Hong, T. Jing, H. Lee, S.N. Kaplan and V. Perez-Mendez, "High efficiency neutron sensitive amorphous silicon pixel detectors," *IEEE Transactions on Nuclear Science*, 41, pp. 915-921, 1994.

[7] D.S. McGregor, J.T. Lindsay, C.C. Brannon and R.W. Olsen, "Semi-insulating bulk GaAs thermal neutron imaging arrays," *IEEE Transactions on Nuclear Science*, 43, pp. 1357-1364, 1996.

[8] C. Petrillo, F. Sacchetti, O. Toket, and N.J. Rhodes, "Solid state neutron detectors," *Nuclear Instruments and Methods*, A378, pp. 541-551, 1996.

[9] F. Foulon, P. Bergonzo, A. Brambilla, C. Jany, B. Guizard and R.D. Marshall, "Neutron detectors made from chemically vapour deposited semiconductors," *Proceedings of the Materials Research Society*, 487, pp. 591-596, 1998.

[10] A.J. Peurrung, "Recent developments in neutron detection," *Nuclear Instruments and Methods*, A443, pp. 400-415, 2000.

[11] H.K. Gersch, D.S. McGregor, and P.A. Simpson, "A study of the effect of incremental gamma-ray doses and incremental neutron fluences upon the performance of self-biased ^{10}B-coated high-purity epitaxial GaAs thermal neutron detectors," *Nuclear Instruments and Methods*, A489, pp. 85-98, 2002.

[12] W.H. Todt, Sr., "Characteristics of self-powered neutron detectors used in power reactors," *Proc. of a Specialists' Meeting on In-core Inst. and Reactor Core Assessment, NEA Nuclear Science Committee*, Mito-shi, Japan, October 1996.

[13] D.S. McGregor, J.K. Shultis, and M. Whaley, "Near-core and in-core neutron radiation monitors for real time neutron flux monitoring and reactor power level measurements," solicitation no. DE-PS03-02SF22467, DOE NERI, 2002.

[14] D.S. McGregor, J.K. Shultis, M.F. Ohmes, A.S.M.S. Ahmed, R. Ortiz, and K. Hoffert, "Micro-Pocket Fission Detectors (MPFD) for Near-Core and In-Core Neutron Flux Monitoring," *Conference Record for the ANS 4th Topical Meeting NPIC & HMIT*, Columbus, Ohio, September 19-22, 2004.

[15] D.S. McGregor, M.F. Ohmes, R.E. Ortiz, A.S.M.S. Ahmed, and J.K. Shultis, "Micro-Pocket Fission Detectors (MPFD) for In-Core Neutron Flux Monitoring," *Nuclear Instruments and Methods,* A554, pp. 494-499, December 2005.

[16] N. Tsoulfanidis, *Measurement and Detection of Radiation*, 2nd ed. Washington, DC: Taylor and Francis, 1995.

[17] Evaluated Nuclear Data File (ENDF), National Nuclear Data Center, Brookhaven National Laboratory, "http://www.nndc.bnl.gov/exfor/endf00.htm", June 12, 2005.

[18] J.M. Harrer and J.G. Beckerley, *Nuclear power reactor instrumentation systems handbook*, volume 1. Oak Ridge, TN: USAEC Technical Information Center, pp. 132-138, 1973.

[19] J. F. Ziegler and J. P. Biersack, SRIM-2003 Code, Version 26, www.srim.org, IBM Company, 2003.

[20] J.K. Shultis and R.E. Faw, "An introduction to the MCNP code," revised April 20, 2005, unpublished.

[21] A. Sharma, "Properties of some gas mixtures used in tracking detectors," SLAC Journal, ICFA, 16, Summer 1998.

[22] A. Bressan, A. Buzulutskov, L. Ropelewski, F. Sauli, and L. Shekhtman, "High gain operation of GEM in pure argon," SLAC Journal, ICFA, 17, Fall 1998.

[23] S.F. Biagi, "Accurate solution of the Boltzmann transport equation," *Nuclear Instruments and Methods in Physics Research*, A273, pp. 533-535, 1988.

[24] R. Johnsen, M.T. Leu, and M.A. Biondi, "Mobilities of mass-identified atomic ions in the noble gases," *Physical Review*, A8(5), pp. 2557-2563, November 1973.

[25] S.C. Brown, *Basic data of plasma physics, 1966*, 2nd Ed, Cambridge, MA: The M.I.T. Press, 1967.

[26] G.D. Bouchey, "Experimental neutron flux measurements and power calibration in the Kansas State University TRIGA Mark II Nuclear Reactor," Thesis Kansas State University, 1967.

[27] S. Glasstone and A. Sesonske, *Nuclear Reactor Engineering*. Malabar, FL: Krieger Publishing Company, 1981.

[28] J.R. Lamarsh, *Introduction to Nuclear Reactor Theory*. LaGrange Park, IL: American Nuclear Society, Inc., 2002.

[29] Kansas State University TRIGA Mark II Nuclear Reactor Facility Training Manual, September 19, 2002.

[30] E.M. Baum, H.D. Knox, and T.R. Miller, *Nuclides and Isotopes, Sixteenth Edition*, KAPL, Inc., 2002.

[31] WISE Uranium Project, "Uranium downblending calculator – help," website "http://www.wise-uranium.org/nfcubh.html," November 25, 2004.

[32] Kansas State University TRIGA Mark II Nuclear Reactor Facility Log Book, January 1999 to May 2005.

[33] E.D. Cullens, "Reactor operation history" (private communication), June 25, 2005.

[34] C.C. Bolinger and T.C.Pinsent (private communication), 2003.

[35] Dupont, "Green Tape", http://www.dupont.com/mcm/product/tape.html, 2003.

[36] K. Hoffert at Reuter Stokes (private communication), 2003.

[37] General Atomics, TRIGA Fuels, website "http://triga.ga.com/fuel.html," August 30, 2005.

[38] H.W. Ott, *Noise Reduction Techniques in Electronic Systems*, 2nd ed. New York: John Wiley & Sons, Inc., 1988.

[39] U.S. DOE Nuclear Energy Research Advisory Committee and Generation IV International Forum, "A technology roadmap for generation IV nuclear energy systems," December 2002.

[40] M.J. Lourenço, J.M. Serra, M.R. Nunes, A.M. Vallêra, and C.A. Nieto de Castro, "Thin-film characterization for high-temperature applications," *International Journal of Thermophysics*, 19(4), pp 1253-1265, 1998.

[41] Aremco Products, Inc., "High temperature ceramic adhesives and pastes, technical bulletin A2," website "http://www.aremco.com/PDFs/A2.pdf," January 2005.

[42] Aremco Products, Inc., "Electrically and thermally conductive materials, technical bulletin A8," website "http://www.aremco.com/PDFs/A8.pdf," January 2005.

[43] Peter Schwartz, Aremco Products, Inc. (private communication), February 2, 2005.